On Numerical Methods for Hyperbolic Conservation Laws and Related Equations Modelling Sedimentation of Solid-Liquid Suspensions

F. Betancourt, R. Bürger, R. Ruiz-Baier, H. Torres, and C.A. Vega

Abstract A classical kinematical model of sedimentation of small equal-sized particles dispersed in a viscous fluid leads to a scalar conservation law with a nonlinear flux. Several extensions of this model are reviewed, with a strong focus on recently developed numerical methods. These extensions include a one-dimensional clarifier-thickener model giving rise to a conservation law with discontinuous flux, a conservation law with nonlocal flux, systems of nonlinear conservation modelling the sedimentation of polydisperse suspensions, and sedimentation-flow models consisting of a conservation law coupled with the Stokes or Navier-Stokes system in two space dimensions. Numerical examples are presented.

F. Betancourt
Departamento de Ingeniería Metalúrgica, Facultad de Ingeniería, Universidad de Concepción, Casilla 160-C, Concepción, Chile
e-mail: fbetancourt@udec.cl

R. Bürger (✉)
CI^{2}MA and Departamento de Ingeniería Matemática, Facultad de Ciencias Físicas y Matemáticas, Universidad de Concepción, Casilla 160-C, Concepción, Chile
e-mail: rburger@ing-mat.udec.cl

R. Ruiz-Baier
Modeling and Scientific Computing, MATHICSE, Ecole Polytechnique Fédérale de Lausanne EPFL, Station 8, CH-1015, Lausanne, Switzerland
e-mail: ricardo.ruiz@epfl.ch

H. Torres
Departamento de Matemáticas, Facultad de Ciencias, Universidad de La Serena, Av. Cisternas 1200, La Serena, Chile
e-mail: htorres@ing-mat.udec.cl

C.A. Vega
Departamento de Matemáticas y Estadística, División de Ciencias Básicas, Universidad del Norte, Barranquilla, Colombia
e-mail: cvega@uninorte.edu.co

G.-Q.G. Chen et al. (eds.), *Hyperbolic Conservation Laws and Related Analysis with Applications*, Springer Proceedings in Mathematics & Statistics 49,
DOI 10.1007/978-3-642-39007-4_2,

2010 Mathematics Subject Classification 65M06, 65M08, 65M60, 76M20, 76T20

1 Introduction

1.1 Scope

The sedimentation of small particles dispersed in a viscous fluid under the influence of a (mostly gravitational) body force is a process of theoretical and practical interest that appears as a controlled unit operation in mineral processing, wastewater treatment, the pulp-and-paper and chemical industry, medicine, volcanology, and other areas where a suspension must be separated into a clarified liquid and concentrated sediment. The particles are small compared with typical length scales (diameter and depth) of the settling vessel. Moreover, sedimentation models for these applications should be able to predict the behaviour of a given unit on relatively large temporal and spatial scales, while microscopical information such as, for instance, the position of a given particle is of little interest. These considerations justify representing the liquid and the solid particles as superimposed continuous phases, namely a liquid phase and one or several solid phases.

The most widely used sedimentation model goes back to Kynch [64], who postulated that (under idealizing circumstances) the settling velocity v_s of a single particle in a batch column is a given function of the local solids volume fraction u only, $v_s = v_s(u)$. Inserting this assumption into the one-dimensional solids continuity equation, written in differential form as

$$u_t + (uv_s)_x = 0, \tag{1}$$

where t is time and x is depth, yields the first-order scalar conservation law

$$u_t + b(u)_x = 0, \quad b(u) := uv_s(u), \tag{2}$$

which is supplied with suitable initial and boundary conditions.

If we assume (for simplicity, but without loss of generality) that u varies between $u = 0$, the clear-liquid limit, and $u = u_{\max}$ with $u_{\max} = 1$ for a packed bed, then a common approach is

$$v_s(u) = v_{St}V(u), \tag{3}$$

where v_{St} is the Stokes velocity, that is, the settling velocity of a single particle in an unbounded fluid, and the so-called hindered settling factor $V = V(u)$ can, for instance, be the one given by Richardson and Zaki [75]

$$V(u) = (1-u)^{n_{RZ}}, \quad n_{RZ} \geq 1, \tag{4}$$

so that $b(u) = u(1-u)^{n_{\mathrm{RZ}}}$. For $n_{\mathrm{RZ}} > 1$, this function has an inflection point $u_{\mathrm{infl}} = 2/(1+n_{\mathrm{RZ}}) \in (0,1)$. Thus, the basic mathematical model is a nonlinear, scalar conservation law with non-convex flux. The precise algebraic form of the batch flux density function $b = b(u)$ is a specific property of the material under consideration.

As it stands, (2) only applies to batch settling of a suspension of small equal-sized (monodisperse) spherical particles. Extensions of (2) have been made, for instance, to include continuously operated so-called clarifier-thickener units, to handle suspensions of particles forming compressible sediments, and to describe polydisperse suspensions with particles having different sizes and densities. Moreover, the dependence of v_{s} on the spot value $u = u(x,t)$ has been replaced by a non-local one, and multi-dimensional versions of (2) have been formulated, which require the solution of additional equations for the motion of the mixture. These extensions give rise to conservation laws with a flux that depends discontinuously on x, strongly degenerate parabolic equations, strongly coupled systems of nonlinear, first-order conservation laws, conservation laws with non-local flux, and multi-dimensional conservation laws coupled with the Stokes or Navier-Stokes system. Thus, the mathematical framework for many sedimentation models relevant to applications includes the well-posedness and numerical analysis of nonlinear hyperbolic conservation laws and related equations. The resulting models have some intriguing non-standard properties that make them interesting objects of study for the well-posedness and numerical analysis of conservation laws and related equations. On the other hand, a thorough understanding of the properties of these models is necessary for the design of reliable numerical simulation tools. This is a particular challenge for clarifier-thickener units. It is the purpose of this contribution to review recent advances in this area.

1.2 Some Historical Remarks and Motivation

To put the original research problem into the proper historical perspective of the engineering application, we first mention that extensive historical accounts are provided in [17, 33]. The exploitation of the difference in density between solid particles and fluid for operations of washing ores can be traced back at least to the ancient Egyptians [94]. The use of settling tanks, operated in a batch or semi-continuous manner, for processes that can now be identified as classification, clarification and thickening, was described in detail in Georgius Agricola's book *De Re Metallica*, first published in 1556 [17, 33]. The most important technological invention that would rationalize the settling process is the continuous thickener, introduced by J.V.N. Dorr, a chemist, cyanide mill owner, consulting engineer and plant designer, in the early twentieth century [44]. A continuous thickener is essentially a cylindrical settling tank into which the feed suspension to be separated is fed continuously, the sediment forming by settling of particles is removed continuously, and the clear liquid produced is removed by a circumferential launder,

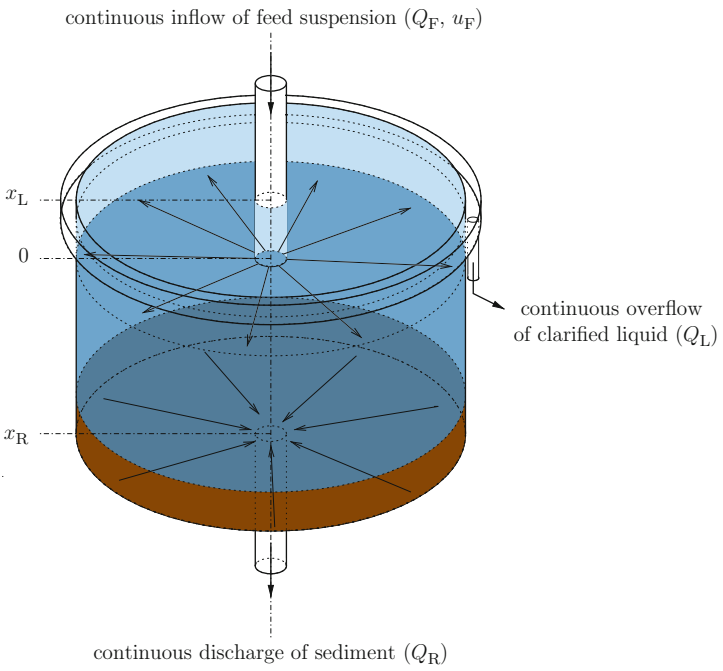

Fig. 1 Schematic view of a clarifier-thickener (CT). Technical details are omitted

see Fig. 1. This design is widely used today in mineral processing and in secondary settling tanks in wastewater treatment.

The invention of the clarifier-thickener was soon followed by efforts to mathematically model its operation. It was recognized early [35] that understanding the dynamics of the batch settling process of a suspension at different solids concentrations is fundamental for effective thickener design and control.

The starting point of the mathematical modelling of sedimentation is the well-known Stokes formula, which states that the settling velocity of a sphere of size (diameter) d and density ρ_s in an unbounded fluid of density ρ_f and viscosity μ_f is given by

$$v_{St} = \frac{g d^2(\rho_s - \rho_f)}{18\mu_f}, \tag{5}$$

where g denotes acceleration of gravity. The settling velocity of a particle in a concentrated suspension is, however, smaller than (5) due to the hindrance exerted by the presence of other particles. This effect can be expressed as an increase in viscosity of the suspension. Explicit formulas describing the phenomenon of hindered settling of the type (3), where the hindered settling factor $V = V(u)$ should satisfy $V(0) = 1$, $V(u_2) < V(u_1)$ for $u_1 < u_2$ and $V(u_{max}) = 0$,

were derived in the dilute limit $u/u_{\max} \ll 1$ more than a century ago by A. Einstein [45], and in the 1940s for both dilute and concentrated suspensions (see, e.g., [55,84,89]). It was in Kynch's specific contribution [64] that he explicitly *solved* the governing equation (1) under the assumption $v_s = v_{St}V(u)$, for initially constant concentrations. In mathematical terms, if the function b has support on the interval $(0, u_{\max})$, then the settling of an initially homogeneous suspension of concentration $u_0 \in (0, u_{\max})$ in a column of depth L can be described by the initial-value problem for (2) defined by the piecewise constant initial datum

$$u(x,0) = \begin{cases} 0 & \text{for } x < 0, \\ u_0 & \text{for } 0 < x < L, \\ u_{\max} & \text{for } x > L \end{cases} \tag{6}$$

corresponding to two adjacent Riemann problems. Kynch [64] applied the method of characteristics and resolving cases of intersection by discontinuities based on physical principles that agree with theoretically motivated entropy conditions to be introduced much later. One piece of insight these constructions could provide is the explanation why fairly dilute and concentrated suspensions would settle with a sharp interface and a zone of continuous transition of concentration separating the growing sediment from the bulk suspension; namely, the former situation gives rise to a kinematic shock (in u) and the latter to a rarefaction.

Kynch's efforts were followed by systematic classifications of qualitatively different solutions to (2) and (6) [51, 90]. Based on work by Ballou [3], K.S. Cheng [34] and Liu [67] (see [33]), Bustos and Concha [32] and Diehl [40] appropiately embedded these constructions into the theory of entropy solutions of a scalar conservation law with non-convex flux. The interest Kynch's theory immediately caused in mineral processing, wastewater treatment (where it has become known as the *solids flux theory*) and other applicative areas has been widely discussed in some reviews (e.g., [17, 42]). Clearly, to make this theory applicable to the settling of a given suspension one must assume that the factor $V = V(u)$ is known. The reliable identification of this factor or equivalently, of the function $b = b(u)$, from experimental data is a current research problem in itself [37,41,50].

The model is very similar to the well-known Lighthill-Whitham-Richards (LWR) model for traffic flow. In fact, in textbooks on hyperbolic conservations, the LWR model forms the preferred example, since the typical flux $b(u) = u(1-u)$ arising in that model is convex and allows for simpler construction of solutions, and the initial value problem (Riemann problem) for such an equation is easier to handle, than for the problem (2) and (6) with b non-convex. The construction of solutions for the direct problem of (2) with piecewise constant initial data and constant u_0 (6) is in any case well understood and for decades has formed standard material for engineering textbooks including [74, 91]. The extensions mentioned in Sect. 1.1 do, however, give rise to research problems centering around the well-posedness and numerical analysis and efficient numerical simulation of the corresponding model.

1.3 Outline of This Contribution

The model for continuous sedimentation was later improved to the configuration of a so-called clarifier-thickener. The basic idea is to replace boundary conditions that would describe feed and discharge operations in a continuously operated unit by changes of the definition of the convective flux. This results in a flux with discontinuities with respect to spatial position, which reflect the injection of feed suspension at a certain level of height into an idealized unit, and the split of the feed flow into upward- and downward-directed bulk flows of the mixture. If sediment compressibility is ignored for the moment, then the resulting model can be expressed as a conservation law with a discontinuous flux:

$$u_t + f\big(\boldsymbol{\gamma}(x), u\big)_x = 0, \quad (x,t) \in \Pi_T := \mathbb{R}, \times (0,T], \tag{7}$$

$$u(x,0) = u_0(x), \quad x \in \mathbb{R}, \tag{8}$$

where $\boldsymbol{\gamma}(x)$ is a given vector of discontinuous parameters. The basic associated difficulty is that well-posedness for (7) is ensured [62] for smooth functions $\boldsymbol{\gamma} = \boldsymbol{\gamma}(x)$, but the theory for discontinuous $\boldsymbol{\gamma} = \boldsymbol{\gamma}(x)$ does *not* emerge as a "limit case" for smooth parameter vectors that approximate a discontinuous one. It turns out that one has to explicitly specify which discontinuities of the solution u are considered to be admissible across the jumps in $\boldsymbol{\gamma}$.

The model was later extended to include the effect of sediment compressibility; the governing equation can then be expressed as

$$u_t + f\big(\boldsymbol{\gamma}(x), u\big)_x = \big(\gamma_2(x) A(u)_x\big)_x, \tag{9}$$

where $\boldsymbol{\gamma} = (\gamma_1, \gamma_2)$ and γ_2 are now discontinuous vectorial and scalar functions, respectively, of x, and $A(\cdot)$ typically has the behaviour

$$A(u) := \int_0^u a(s)\,\mathrm{d}s, \quad a(u) \begin{cases} = 0 & \text{for } u \le u_c, \\ > 0 & \text{for } u > u_c, \end{cases} \quad u_c > 0, \tag{10}$$

where u_c is a critical concentration above which the solid particles touch each other.

The well-posedness analysis of the model (7) or (9), together with (8), has been a small part of the tremendous interest and activity conservation laws and related equations with dicontinuous flux have seen in recent years. Partial overviews are given in [16, 23], while a comprehensive and unifying treatment is provided by Andreianov, Karlsen, and Risebro [2]. While some of the previous existence results are based on the convergence of suitable monotone, and therefore first-order, finite difference schemes (cf., e.g., [19–21, 23, 25, 59, 88] and [60] for the underlying L^1 stability theory), it is desirable for practical purposes to construct higher order schemes, for examples analogues to second-order TVD schemes for standard conservation laws, for which one would be able to prove convergence

at least to a weak solution. In Sect. 2, which summarizes results of [25], two different methodologies to construct a simple TVD scheme and a flux-TVD scheme, respectively, are illustrated, along with an outline of the convergence analysis for the flux-TVD scheme that is based on a nonlocal flux limiter algorithm.

In Sect. 3 we study the family of conservation laws with nonlocal flux

$$u_t + \big(u(1-u)^\alpha V(K_a * u)\big)_x = 0, \quad x \in \mathbb{R}, \quad t \in (0,T], \tag{11}$$

together with the initial datum

$$u(0,x) = u_0(x), \quad 0 \le u_0(x) \le 1, \quad x \in \mathbb{R}, \tag{12}$$

where either $\alpha = 0$ or $\alpha \ge 1$. Usually, one defines a kernel $K = K(x)$ with support on $[-2,2]$ and sets $K_a(x) := a^{-1}K(a^{-1}x)$ with support on $[-2a,2a]$. The basic motivation of the nonlocal dependence (34) lies in the observation that Kynch's theory, despite being a useful approximation, sharply contrasts with the theoretical result that the velocity of each particle is determined by the size and position of all spheres and the nature of possible boundaries. The convolution of u with a weighting function, an assumption that eventually leads to (34) (see [12]), is a compromise.

In [12] the well-posedness of (11) and (12) is studied. The main results are the uniqueness and existence of entropy solutions. This is done by proving convergence of a difference-quadrature scheme based on the standard Lax-Friedrichs scheme. It turns out that for $\alpha = 0$, solutions are bounded by a constant that depends on the final time T, and are Lipschitz continuous if u_0 is Lipschitz continuous. In contrast, for $\alpha \ge 1$ solutions are in general discontinuous even if u_0 is smooth, but assume values within the interval $[0,1]$ for all times. Some numerical examples illustrate the solution behaviour, in particular the so-called effect of layering in sedimenting suspensions and the differences between the cases $\alpha = 0$ and $\alpha \ge 1$. These results are summarized in Sect. 3.

Next, in Sect. 4, we will consider models of sedimentation of polydisperse suspensions. These mixtures consist of small solid particles that belong to a number N of species that may differ in size or density, and which are dispersed in a viscous fluid. Here we only consider particles of the same density. If ϕ_i denotes the volume fraction of particle species i having diameter D_i, where we assume that $D_1 > D_2 > \cdots > D_N$, and v_i is the phase velocity of species i, then the continuity equations of the N species are $\partial_t \phi_i + \partial_x(\phi_i v_i) = 0$, where t is time and x is depth. (In this section any statement involving a free index i is supposed to hold for $i = 1,\dots,N$.) The velocities v_i are assumed to be given functions of the vector $\Phi := \Phi(x,t) := (\phi_1(x,t),\dots,\phi_N(x,t))^{\mathrm{T}}$ of local concentrations. This yields nonlinear, strongly coupled systems of conservation laws of the type

$$\partial_t \Phi + \partial_x \boldsymbol{f}(\Phi) = 0, \quad \boldsymbol{f}(\Phi) := \big(f_1(\Phi),\dots,f_N(\Phi)\big)^{\mathrm{T}}, \quad f_i(\Phi) := \phi_i v_i(\Phi). \tag{13}$$

We seek solutions $\Phi = \Phi(x,t)$ that take values in the closure of the set

$$\mathcal{D}_{\phi_{\max}} := \left\{\Phi \in \mathbb{R}^N \,:\, \phi_1 > 0, \ldots, \phi_N > 0,\, \phi := \phi_1 + \cdots + \phi_N < \phi_{\max}\right\}.$$

The parameter $0 < \phi_{\max} \leq 1$ is a given maximum solids concentration. For batch settling in a column of height L, (13) is defined on $\Omega_T := \{(x,t) \in \mathbb{R}^2 \,|\, 0 \leq x \leq L,\ 0 \leq t \leq T\}$ for a given final time $T > 0$ along with the initial condition

$$\Phi(x,0) = \Phi^0(x) = \left(\phi_1^0(x), \ldots, \phi_N^0(x)\right)^{\mathrm{T}}, \quad \Phi^0(x) \in \bar{\mathcal{D}}_{\phi_{\max}}, \quad x \in [0,L]$$

and the zero-flux boundary conditions

$$\boldsymbol{f}\,|_{x=0} = \boldsymbol{f}\,|_{x=L} = 0. \tag{14}$$

Several choices of v_i ("models") as functions of Φ, and depending on the vector of normalized particle sizes $\boldsymbol{d} := (d_1, \ldots, d_N)^{\mathrm{T}}$, where $d_i := D_i/D_1$, have been proposed [96]. We here discuss the models due to Masliyah [68] and Lockett and Bassoon [65] (the "MLB model") and Höfler and Schwarzer [56] (the "HS model"), respectively. Both models are strictly hyperbolic for all $\Phi \in \mathcal{D}_{\phi_{\max}}$, for arbitrary N, and under certain restrictions on model parameters and d_N [24]. We mention here that hyperbolicity for a large range of parameter values is a desirable property for polydisperse sedimentation models with equal-density particles, since such mixtures have been observed to always settle stably, i.e., under the formation of horizontal layers and interfaces. Instabilities, such as the formation of blobs and columns, have been observed with particles having different densities only [93], and their ocurrence is predicted by a criterion equivalent to loss of hyperbolicity [6, 18].

In Sect. 4 the main results of [26] are summarized. Specifically, the results in [24] provide a good estimate of the viscosity coefficient in a Lax-Friedrichs-type flux splitting. This allows one to construct high-resolution component-wise weighted essentially non-oscillatory (WENO) schemes (cf. [79] and its references) for the numerical solution of (13)–(14). In addition, the full spectral decomposition of $\mathcal{J}_f(\Phi)$, which can now be computed numerically, can be used to obtain *characteristic-based* WENO schemes, for which the WENO reconstruction procedure is applied to the local characteristic variables and fluxes at each cell-interface. When combined with a strong stability preserving (SSP) Runge-Kutta-type time discretization (see [49]), the resulting SSP-WENO-SPEC schemes turn out to be extremely robust. Here we summarize results related to the hyperbolicity analysis and the construction of the aforementioned schemes, and present some numerical examples.

In Sect. 5 we are concerned with the simulation of sedimentation of monodisperse suspensions in several space dimensions. In fact, for the realistic description of the sedimentation of suspensions in two- or three-dimensional (2D, 3D) domains the governing system of PDEs is a (possibly degenerate) convection-diffusion equation

coupled with a version of the Stokes or Navier-Stokes system, supplied with suitable initial and boundary conditions.

A prototype model of this kind is given by the following system, where the local solids concentration u, the mixture velocity $\boldsymbol{v}$ and the pressure p are sought:

$$u_t + \nabla \cdot (u\boldsymbol{v} + f(u)\boldsymbol{k}) = \Delta A(u), \quad \boldsymbol{x} \in \Omega \subset \mathbb{R}^d, \quad t \in (0, T], \tag{15}$$

$$\begin{aligned} \nu(\rho_s u + \rho_f(1-u))(\boldsymbol{v}_t + \boldsymbol{v} \cdot \nabla \boldsymbol{v}) - \nabla \cdot \big(\mu(u)\nabla \boldsymbol{v}\big) + \lambda \nabla p = \zeta u \boldsymbol{k}, \\ \nabla \cdot \boldsymbol{v} = 0, \end{aligned} \tag{16}$$

where $d = 2$ or 3, $f(u) = uV(u)$, $\boldsymbol{k}$ is the upwards-pointing unit vector, the term $\Delta A(u)$ accounts for sediment compressibility where the integrated diffusion coefficient $A(\cdot)$ has the behaviour (10), $\mu(u)$ is a viscosity function, and $\nu \geq 0$, $\zeta > 0$ and $\lambda > 0$ are constants. Note that the convection-diffusion equation (15) involves the linear transport term $u\boldsymbol{v}$, while $\boldsymbol{v}$ (and p) are determined by the Navier-Stokes or Stokes (for $\nu > 0$ and $\nu = 0$, respectively) system (16). This strong coupling of (15) and (16) is the main challenge for solving this sedimentation-flow model. The equations (16) do not have to be solved in a 1D setting, since then $v_x = 0$, so in absence of sources or sinks, $v = v(t)$ becomes controllable. We present numerical results for two-dimensional subcases of (15) and (16) discretized either by finite volume schemes combinded with an adaptive multiresolution technique or by a finite volume element scheme.

Some open research problems and alternate treatments are discussed in Sect. 6.

2 TVD and Flux-TVD Schemes for Clarifier-Thickener Models

2.1 Clarifier-Thickener Models

The basic principle of operation of a clarifier-thickener can be inferred from Fig. 1. The feed suspension, which is to be separated into a concentrated sediment and a clarified liquid, is fed into a cylindrical vessel at depth level $x = 0$, at a volume rate $Q_F \geq 0$ and with a feed solids volume fraction $u_F \geq 0$. The feed flow immediately spreads over the whole cross section, and is separated into upward- and downward-directed bulk flows forming the so-called clarification and thickening zones $x_L < x < 0$ and $0 < x < x_R$, respectively. The solid particles settle downward, forming a concentrated sediment at the bottom which is continuously removed at a controllable discharge volume rate $Q_R \geq 0$, while the overflowing supernatant liquid is collected in a circumferential launder. The (signed) liquid overflow rate is $Q_L \leq 0$, such that $Q_F = Q_R - Q_L$. We assume that solid-liquid separation takes place within the unit only, but not in the overflow and discharge flows, where both phases move with the

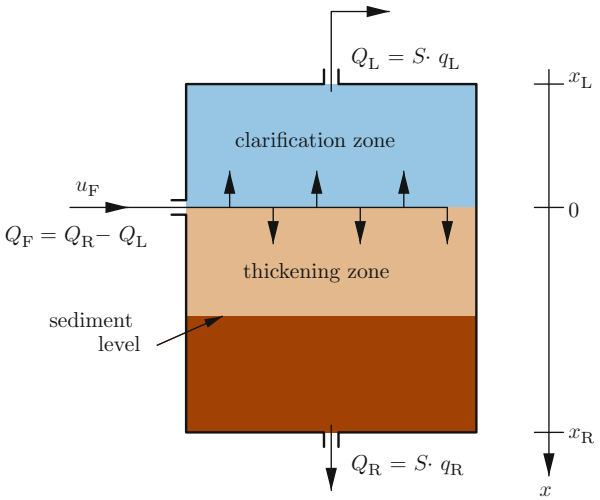

Fig. 2 One-dimensional idealized clarifier-thickener model

same speed. In applications, real-world units usually have a gently sloped bottom; however in this review we assume that the cross-sectional area S is constant.

If we assume that all flow variables are horizontally constant and wall effects are negligible, then the conceptual model reduces to the setup shown in Fig. 2. To derive the final mathematical model, we replace the solids and fluid phase velocities v_s and v_f by the volume average velocity of the mixture, $q := uv_s + (1-u)v_f$ and the solid-fluid relative velocity $v_r = v_s - v_f$. One then always has $q_x = 0$, i.e. $q = q(t)$ in the absence of sources and sinks, and $v_s = q + (1-u)v_r$. In particular, $q = 0$ for settling in a closed column. For the clarifier-thickener model of Fig. 2, the velocities q_R, q_L and q_F are related to the signed volume bulk flows by $q_R = Q_R/S$, $q_L = Q_L/S$ and $q_F = Q_F/S$. Moreover, stating the constitutive assumption as

$$v_r(u) = \frac{b(u)}{u(1-u)},$$

we obtain the governing equation (7), where

$$f\big(\boldsymbol{\gamma}(x), u\big) = \gamma_1(x)b(u) + \gamma_2(x)(u - u_F).$$

The parameters γ_1 and γ_2 are defined as follows, and discriminate between the interior and exterior of the unit and the directions of the bulk flows, respectively:

$$\gamma_1(x) := \begin{cases} 1 & \text{for } x \in (x_L, x_R), \\ 0 & \text{for } x \notin (x_L, x_R)\,, \end{cases} \qquad \gamma_2(x) := \begin{cases} q_L & \text{for } x < 0, \\ q_R & \text{for } x > 0. \end{cases} \tag{17}$$

If we include the effect of sediment compressibility, then the governing equation is given by (9), where γ_1 and γ_2 are still given by (17).

By a solution to the hyperbolic problem (7) and (8) we understand the following, where BV_t denotes the space of locally integrable functions on Π_T for which u_t (but not u_x) is a locally bounded measure, which is a superset of BV.

Definition 1 (BV_t weak solution). A measurable function $u : \Pi_T \to \mathbb{R}$ is a BV_t weak solution of (7) and (8) if $u \in (L^\infty \cap BV_t)(\Pi_T)$, and if for all test functions $\phi \in \mathcal{D}(\mathbb{R} \times [0, T))$,

$$\iint_{\Pi_T} \Big(u\phi_t + f\big(\boldsymbol{\gamma}(x), u\big)\phi_x \Big)\, dx\, dt + \int_{\mathbb{R}} u_0 \phi(x, 0)\, dx = 0.$$

2.2 TVD and Flux-TVD (FTVD) Schemes

We start with a description of the scheme under study in general form, and identify terms that ensure that the resulting scheme has second order accuracy. To this end we consider the case $A \equiv 0$ and select $\Delta x > 0$ and set $x_j := j\Delta x$, $\boldsymbol{\gamma}_{j+1/2} := \boldsymbol{\gamma}(x_{j+1/2}+)$ and $U_j^0 := u_0(x_j+)$ for $j \in \mathbb{Z}$. Here $x_{j+1/2} := x_j + \Delta x/2$. Let $t_n := n\Delta t$ and let χ^n denote the characteristic function of $[t_n, t_{n+1})$, χ_j the characteristic function of $[x_{j-1/2}, x_{j+1/2})$, and $\chi_{j+1/2}$ the characteristic function of the interval $[x_j, x_{j+1})$. Our difference algorithm will produce an approximation U_j^n associated with (x_j, t_n). We then define

$$u^\Delta(x,t) := \sum_{n\geq 0}\sum_{j\in\mathbb{Z}} U_j^n \chi_j(x)\chi^n(t), \quad \boldsymbol{\gamma}^\Delta(x) := \sum_{j\in\mathbb{Z}} \boldsymbol{\gamma}_{j+1/2}\chi_{j+1/2}(x). \tag{18}$$

We recall the definition of the standard difference operators $\Delta_- V_j := V_j - V_{j-1}$ and $\Delta_+ V_j := V_{j+1} - V_j$. Then our algorithm is defined by

$$U_j^{n+1} = U_j^n - \lambda\Delta_-\big(h_{j+1/2}^n + \hat{F}_{j+1/2}^n\big), \quad \lambda = \frac{\Delta t}{\Delta x}, \quad j \in \mathbb{Z}, \quad n = 0, 1, 2, \ldots. \tag{19}$$

Here $h_{j+1/2}^n := h(\boldsymbol{\gamma}_{j+1/2}, U_{j+1}^n, U_j^n)$, where h is the Engquist-Osher (EO) flux [46]:

$$h(\boldsymbol{\gamma}, v, u) := \frac{1}{2}\big(f(\boldsymbol{\gamma}, u) + f(\boldsymbol{\gamma}, v)\big) - \frac{1}{2}\int_u^v \big|f_u(\boldsymbol{\gamma}, w)\big|\, dw, \tag{20}$$

and $\hat{F}_{j+1/2}^n$ is a correction term that is required in order to achieve second-order accuracy. Without those terms, (19) is the first-order scheme analyzed in [20]. Finally, we keep λ constant as we refine the mesh.

Focusing on the difference scheme (19) for (7), we now define second-order correction terms $d^n_{j+1/2}$, $e^n_{j+1/2}$ that are appropriate if $\boldsymbol{\gamma}$ is piecewise constant. We are seeking formal second-order accuracy at points (x,t) where the solution u is smooth. At jumps in $\boldsymbol{\gamma}$, u will generally be discontinuous, so for the purpose of defining correction terms, we concentrate on points located away from the jumps in $\boldsymbol{\gamma}$. In light of our (temporary) assumption that $\boldsymbol{\gamma}$ is piecewise constant we obtain the following Lax-Wendroff type correction terms that are well known to provide for formal second-order accuracy in both space and time (see e.g. [86]):

$$d^n_{j+1/2} = \frac{\alpha^+_{j+1/2}}{2}\big(1-\lambda\alpha^+_{j+1/2}\big)\Delta_+ U^n_j, \quad e^n_{j+1/2} = \frac{\alpha^-_{j+1/2}}{2}\big(1+\lambda\alpha^-_{j+1/2}\big)\Delta_+ U^n_j. \tag{21}$$

Here the quantities $\alpha^\pm_{j+1/2}$ are the positive and negative wave speeds associated with the cell boundary located at $x_{j+1/2}$:

$$\alpha^+_{j+1/2} := \frac{1}{\Delta_+ U^n_j}\int_{U^n_j}^{U^n_{j+1}} \max\big(0, f_u(\boldsymbol{\gamma}_{j+1/2}, w)\big)\,\mathrm{d}w = \frac{f(\boldsymbol{\gamma}_{j+1/2}, U^n_{j+1}) - h^n_{j+1/2}}{\Delta_+ U^n_j} \geq 0,$$

$$\alpha^-_{j+1/2} := \frac{1}{\Delta_+ U^n_j}\int_{U^n_j}^{U^n_{j+1}} \min\big(0, f_u(\boldsymbol{\gamma}_{j+1/2}, w)\big)\,\mathrm{d}w = \frac{h^n_{j+1/2} - f(\boldsymbol{\gamma}_{j+1/2}, U^n_j)}{\Delta_+ U^n_j} \leq 0.$$

The scheme defined by (19) and (20), and with the flux correction terms not in effect, i.e., $\hat{F}^n_{j+1/2} = 0$ for all j and n, is only first-order accurate. We now set out to find second-order correction terms that are required when $x \mapsto \boldsymbol{\gamma}(x)$ is piecewise C^2, and start by identifying the truncation error of the first-order scheme. For the case $f_u(\boldsymbol{\gamma}, u) \geq 0$ the first-order version of the scheme (19) simplifies to

$$U^{n+1}_j - U^n_j + \lambda\Delta_- f\big(\boldsymbol{\gamma}_{j+1/2}, U^n_j\big) = 0.$$

Inserting a smooth solution $u(x,t)$ into this scheme, using u^n_j to denote $u(x_j, t^n)$, substituting $u_t = -f(\boldsymbol{\gamma}, u)_x$ into the resulting expression (as well as differentiated versions of this identity) and applying Taylor expansions, we get (see [25] for details)

$$TE^+ = -\Delta x^2\lambda\left[\frac{1}{2}f_u(1-\lambda f_u)u_x - \frac{1}{2}\lambda f_u f_{\boldsymbol{\gamma}}\boldsymbol{\gamma}_x\right]_x + \mathcal{O}(\Delta^3).$$

Similarly, when $f_u \leq 0$, we arrive at the following formula for the truncation error:

$$TE^- = \Delta x^2\lambda\left[\frac{1}{2}f_u(1+\lambda f_u)u_x + \frac{1}{2}\lambda f_u f_{\boldsymbol{\gamma}}\boldsymbol{\gamma}_x\right]_x + \mathcal{O}(\Delta^3).$$

So, when $\boldsymbol{\gamma}$ is piecewise smooth (not piecewise constant), we see from these expressions that appropriate second-order correction terms are given by the following modified versions of (21):

$$\begin{aligned} F^n_{j+1/2} &:= D^n_{j+1/2} - E^n_{j+1/2}, \\ D^n_{j+1/2} &:= d^n_{j+1/2} - \frac{1}{2}\lambda\alpha^+_{j+1/2} f_{\boldsymbol{\gamma}}\big(\boldsymbol{\gamma}_{j+1/2}, U^n_{j+1/2}\big)\Delta_+\boldsymbol{\gamma}_j, \\ E^n_{j+1/2} &:= e^n_{j+1/2} + \frac{1}{2}\lambda\alpha^-_{j+1/2} f_{\boldsymbol{\gamma}}\big(\boldsymbol{\gamma}_{j+1/2}, U^n_{j+1/2}\big)\Delta_+\boldsymbol{\gamma}_j. \end{aligned} \tag{22}$$

For the values $f_{\boldsymbol{\gamma}}(\boldsymbol{\gamma}_{j+1/2}, U^n_{j+1/2})$ appearing in (22), we use the approximation

$$f_{\boldsymbol{\gamma}}(\boldsymbol{\gamma}_{j+1/2}, U^n_{j+1/2}) \approx \frac{1}{2}\big(f_{\boldsymbol{\gamma}}(\boldsymbol{\gamma}_{j+1/2}, U^n_j) + f_{\boldsymbol{\gamma}}(\boldsymbol{\gamma}_{j+1/2}, U^n_{j+1})\big). \tag{23}$$

Even without the jumps in $\boldsymbol{\gamma}$, the solution will generally develop discontinuities. If we use the correction terms above without further processing, the solution will develop spurious oscillations near these discontinuities. To damp out the oscillations, we apply so-called flux limiters, resulting in the flux-limited quantities $\hat{F}_{j+1/2}$.

A simple limiter that enforces the TVD property when $\boldsymbol{\gamma}$ is constant is

$$\begin{aligned} \hat{F}^n_{j+1/2} &= \hat{D}^n_{j+1/2} - \hat{E}^n_{j+1/2}, \\ \hat{D}^n_{j+1/2} &= \operatorname{minmod}\big(D^n_{j+1/2}, 2D^n_{j-1/2}\big), \\ \hat{E}^n_{j+1/2} &= \operatorname{minmod}\big(E^n_{j+1/2}, 2E^n_{j+3/2}\big), \end{aligned} \tag{24}$$

where we recall that the m-variable minmod function is defined by

$$\operatorname{minmod}(p_1, \ldots, p_m) = \begin{cases} \min\{p_1, \ldots, p_m\} & \text{if } p_1 \geq 0, \ldots, p_m \geq 0, \\ \max\{p_1, \ldots, p_m\} & \text{if } p_1 \leq 0, \ldots, p_m \leq 0, \\ 0 & \text{otherwise.} \end{cases}$$

When $\boldsymbol{\gamma}$ is not constant, the actual solution u is not TVD, but numerical experiments [25] indicate that (24) is an effective method of damping oscillations even in the variable-$\boldsymbol{\gamma}$ context considered here. The only negative practical aspect that we have observed is a small amount of overshoot in certain cases when a shock collides with a stationary discontinuity at a jump in $\boldsymbol{\gamma}$, see Fig. 4.

Next, we wish to eliminate the non-physical overshoot observed with the simple TVD limiter (24), and also put the resulting difference scheme on a firm theoretical basis. For a conservation law having a flux with a discontinuous spatial dependency, it is natural to expect not the conserved variable, but the flux, to be TVD [88]. Consequently, we require that

$$\sum_{j\in\mathbb{Z}}\left|\Delta_+ h^{n+1}_{j-1/2}\right| \le \sum_{j\in\mathbb{Z}}\left|\Delta_+ h^{n}_{j-1/2}\right|, \quad n = 0, 1, \ldots.$$

We call this property flux-TVD, or FTVD. We will see that under an appropriate CFL condition, the FTVD property (along with a bound on the solution) holds if

$$\left|\Delta_+ \hat{F}^n_{j+1/2}\right| \le \left|\Delta_+ h^n_{j+1/2}\right|, \quad j \in \mathbb{Z}, \quad n = 0, 1, 2, \ldots. \tag{25}$$

It is reasonable to also impose the condition

$$0 \le \hat{F}^n_{j+1/2}/F^n_{j+1/2} \le 1, \quad j \in \mathbb{Z}, \quad n = 0, 1, 2, \ldots. \tag{26}$$

in addition to (25), so that after we have applied the correction terms, the numerical flux lies somewhere between the first-order flux and the pre-limiter version of the second-order flux.

We can view (25) and (26) as a system of inequalities, and ask if it is possible to find a solution that keeps the ratio $\hat{F}^n_{j+1/2}/F^n_{j+1/2}$ appearing in (26) close enough to unity that we still have formal second-order accuracy. This leads us to propose the nonlocal limiter algorithm that we describe in Algorithm 1.

For the case of piecewise constant $\boldsymbol{\gamma}$, the results produced by the two algorithms (namely the "simple TVD scheme" (STVD) and the "flux-TVD scheme" (FTVD)) usually differ by only a small amount. However, we have observed one situation where there is a discernable difference—the case of a shock impinging on a discontinuity in $\boldsymbol{\gamma}$. As mentioned above, the STVD limiter sometimes allows overshoots by a small amount in this situation. We have not observed any such overshoot with the FTVD limiter, see Example 2 in Sect. 2.3.

Finally, we mention that at a steady sonic rarefaction, both the Engquist-Osher (EO) scheme and the Godunov scheme are slightly overcompressive, leading to a so-called dogleg feature in the solution. This feature vanishes as the mesh size tends to zero, but it is distracting. This dogleg artifact is present in certain situations with both the STVD and the FTVD versions of our second-order schemes. It turns out that if the corrections (21) are replaced by

$$d^n_{j+1/2} = \frac{1}{2}\alpha^+_{j+1/2}\left(\frac{\alpha^+_{j+1/2}}{\alpha^+_{j+1/2} - \alpha^-_{j+1/2}} - \lambda\alpha^+_{j+1/2}\right)\Delta_+ U^n_j,$$

$$e^n_{j+1/2} = \frac{1}{2}\alpha^-_{j+1/2}\left(-\frac{\alpha^-_{j+1/2}}{\alpha^+_{j+1/2} - \alpha^-_{j+1/2}} + \lambda\alpha^-_{j+1/2}\right)\Delta_+ U^n_j,$$

the scheme only changes near sonic points, but the dogleg feature diminishes noticeably. We have implemented this refinement in Examples 1–3.

Next, we describe a method for solving the system of inequalities (25) and (26) while trying to maximize $\hat{F}^n_{j+1/2}/F^n_{j+1/2}$ to maintain formal second-order accuracy wherever possible. We set $z_i := F^n_{i+1/2}$, $\theta_i := |\Delta_+ h^n_{i+1/2}|$ and $\hat{z}_i := \hat{F}^n_{i+1/2}$, and then restate the system of inequalities (25) and (26) in the form

$$|\hat{z}_{i+1} - \hat{z}_i| \le \theta_i, \quad 0 \le \hat{z}_i / z_i \le 1. \tag{27}$$

The unknowns are $\hat{z}_i$, and the data are z_i, $\theta_i \ge 0$. Moreover, there are indices i_*, i^* such that $z_i = 0$ for $i \le i_*$ and $i \ge i^*$ since u_0 has compact support. Thus we may always assume that U_j^n and $F_{j+1/2}^n$ vanish for sufficiently; large j.

Algorithm 1 (Nonlocal limiter algorithm).
Input: data $z_i \ge 0$, $\theta_i \ge 0$, $i = i_*, \ldots, i^*$.
Output: a vector $\hat{Z} = \{\hat{z}_{i_*}, \ldots, \hat{z}_{i^*}\}$ *such that* (27) *is satisfied, where* z_i *denotes the data before application of the algorithm.*
Initialization: The sequence $\zeta_i \ge 0$, $\theta_i \ge 0$, $i = i_*, \ldots, i^*$ *is initialized to the input data* $z_i \ge 0$, $\theta_i \ge 0$, $i = i_*, \ldots, i^*$.

1. *Preprocessor step:*

do $i = i_*, i_* + 1, \ldots, i^* - 1$

if $\zeta_{i+1}\zeta_i < 0$ ***and*** $|\zeta_{i+1} - \zeta_i| > \theta_i$ ***then***

$\zeta_i \leftarrow \operatorname{sgn}(\zeta_i) \min\{|\zeta_i|, \theta_i/2\}$
$\zeta_{i+1} \leftarrow \operatorname{sgn}(\zeta_{i+1}) \min\{|\zeta_{i+1}|, \theta_i/2\}$

endif

enddo

2. *Forward sweep:*

do $i = i_*, i_* + 1, \ldots, i^* - 1$

if $|\zeta_{i+1}| > |\zeta_i|$ ***then***

$\zeta_{i+1} \leftarrow \zeta_i + \operatorname{sgn}(\zeta_{i+1} - \zeta_i) \min\{|\zeta_{i+1} - \zeta_i|, \theta_i\}$

endif

enddo

3. *Backward sweep:*

do $i = i^*, i^* - 1, \ldots, i_* + 1$

if $|\zeta_{i-1}| > |\zeta_i|$ ***then***

$\zeta_{i-1} \leftarrow \zeta_i + \operatorname{sgn}(\zeta_{i-1} - \zeta_i) \min\{|\zeta_{i-1} - \zeta_i|, \theta_{i-1}\}$

endif

enddo

Generate output:

do $i = i_*, i_* + 1, \ldots, i^*$

$\hat{z}_i \leftarrow \zeta_i$

enddo

Here the left arrow $\leftarrow$ is the replacement operator. Algorithm 1 can be written compactly as $\hat{Z} = \Phi(Z, \Theta) = \Phi^-(\Phi^+(\tilde{Z}, \Theta), \Theta)$, where $\tilde{Z} = \text{Pre}(Z, \Theta)$. Here Φ^+ and Φ^- represent the forward and backward sweeps, Pre represents the preprocessor step, and $\hat{Z} = \{\hat{z}_i\}$, $\tilde{Z} = \{\tilde{z}_i\}$, $Z = \{z_i\}$ and $\Theta = \{\theta_i\}$. In [25] it is shown that the output of Algorithm 1 solves the system of inequalities (27), and that the limiter Φ is consistent with formal second-order accuracy in the following sense.

Lemma 1. *Let u and $\boldsymbol{\gamma}$ be C^2 in a neighborhood of the point $\bar{x}$ where*

$$f\big(\boldsymbol{\gamma}(\bar{x}), u(\bar{x})\big)_x \neq 0. \tag{28}$$

Assume that $u(\pm x) = u_{\pm\infty}$ for x sufficiently large, so that the limiter Φ is well-defined on the flux corrections $F^{\Delta}_{j+1/2} = F_{j+1/2}$. Let

$$\hat{F}^{\Delta} = \Phi\left(\left\{F^{\Delta}_{j+1/2}\right\}_{j\in\mathbb{Z}}, \left\{\left|\Delta_+ h_{j+1/2}\right|\right\}_{j\in\mathbb{Z}}\right). \tag{29}$$

Then there is a mesh size $\Delta_0 = \Delta_0(\bar{x}) > 0$ and a $\delta(\bar{x}) > 0$ such that for $\Delta \leq \Delta_0$, we have

$$\hat{F}^{\Delta}_{j+1/2} = F^{\Delta}_{j+1/2} \quad \textit{for all } x_j \in \{x : |x - \bar{x}| < \delta\}.$$

Consequently, the scheme defined by (18)–(23), including the flux corrections $\hat{F}^n_{j+1/2}$ produced by (29) will have formal second-order accuracy at any point where u andγ are smooth, and where (28) is satisfied. Thus, the resulting FTVD scheme is given by $U^{n+1}_j = U^n_j - \lambda\Delta_-(h^n_{j+1/2} + \hat{F}^n_{j+1/2})$. In [20] the first-order version of this scheme, $U^{n+1}_j = U^n_j - \lambda\Delta_- h^n_{j+1/2}$, was analyzed. Clearly, this scheme results by setting $\hat{F}^n_{j+1/2} = 0$ for all j and n. Moreover in [20] we assumed that $\boldsymbol{\gamma}$ is piecewise constant, while in [19] we dealt with a piecewise smooth coefficient function $\boldsymbol{\gamma}$. The convergence analysis for the FTVD scheme strongly relies on results from [19] and [20]. We assume that the following CFL condition is satisfied:

$$\lambda\Big(\max\{-q_{\text{L}}, q_{\text{R}}\} + \|\gamma_1 b'\|\Big) \leq \frac{1}{4}, \tag{30}$$

where $\|\gamma_1 b'\| := \max\{|\gamma_1(x)b'(u)| : x \in [x_{\text{L}}, x_{\text{R}}],\ u \in [0, u_{\max}]\}$.

Our theorem concerning convergence is the following.

Theorem 1 (Convergence of the FTVD scheme). *Let u^{Δ} be defined by (18)–(23). Assume that the flux corrections $\hat{F}^n_{j+1/2}$ are produced by applying Algorithm 1 to the non-limited flux corrections $F^n_{j+1/2}$. Let $\Delta \to 0$ with λ constant and the CFL condition (30) be satisfied. Then u^{Δ} converges along a subsequence in $L^1_{\text{loc}}(\Pi_T)$ and boundedly a.e. in Π_T to a BV_t weak solution of the CT model (7) and (8).*

The proof of Theorem 1 amounts to checking that Lemmas 1–7, along with the relevant portion of Theorem 1, of [19] remain valid in the present context. See [25] for details. We resume the essential steps of the proof.

One first shows that under the CFL condition (30) we get a uniform bound on U_j^n, specifically $U_j^n \in [0,1]$, and that the flux-TVD property is satisfied, i.e.,

$$\sum_{j\in\mathbb{Z}} \left|h_{j+1/2}^{n+1} - h_{j-1/2}^{n+1}\right| \le \sum_{j\in\mathbb{Z}} \left|h_{j+1/2}^{n} - h_{j-1/2}^{n}\right|, \quad n = 0,1,2,\ldots.$$

The proof of these properties follows that of [19, Lemma 1].

The flux-TVD property is the ingredient that allows us to maintain time continuity even though the present scheme, as a second-order scheme, is no longer monotone. Thus, there exists a constant C, independent of Δ and n, such that

$$\Delta x \sum_{j\in\mathbb{Z}} \left|U_j^{n+1} - U_j^n\right| \le \Delta x \sum_{j\in\mathbb{Z}} \left|U_j^1 - U_j^0\right| \le C\Delta t.$$

As in [19], to prove that the difference scheme converges, one needs to establish compactness for the transformed quantity z^Δ that emerges from the numerical solution by a singular mapping Ψ also known as the Temple functional [87]. The critical ingredient is a bound on its total variation. We then derive compactness for u^Δ by appealing to the monotonicity and continuity of the mapping $u \mapsto \Psi(\boldsymbol{\gamma}, u)$. To show that z^Δ has bounded variation it then suffices to invoke Lemmas 2–7 of [19], making modifications where necessary to account for the addition of the second-order correction terms. See [25].

We now use the notation $\mathcal{O}(\Delta\boldsymbol{\gamma}_j)$ to denote terms which sum (over j) to $\mathcal{O}(|\boldsymbol{\gamma}|_{BV})$, and employ the Kružkov entropy-entropy flux pair indexed by c, i.e. $q(u) := |u-c|$ and $\eta(\boldsymbol{\gamma}, u) := \operatorname{sgn}(u-c)(f(\boldsymbol{\gamma}, u) - f(\boldsymbol{\gamma}, c))$. One then obtains that for each $c \in \mathbb{R}$, the following inequality holds:

$$\begin{aligned} q\big(U_j^{n+1}\big) \le q\big(U_j^n\big) - \lambda\Big[H\big(\boldsymbol{\gamma}_{j+1/h}, U_{j+1}^n, U_j^n\big) - H\big(\boldsymbol{\gamma}_{j+1/h}, U_j^n, U_{j-1}^n\big)\Big] \\ + \lambda\left|\Delta_+ h_{j-1/2}^n\right| + \lambda\mathcal{O}(\Delta\boldsymbol{\gamma}_j), \quad j \in \mathbb{Z}, \quad n = 0,1,2\ldots, \end{aligned} \tag{31}$$

where the EO numerical entropy flux is given by

$$H(\gamma, v, u) = \frac{1}{2}\big(\eta(\boldsymbol{\gamma}, u) + \eta(\boldsymbol{\gamma}, v)\big) - \frac{1}{2}\int_u^v \operatorname{sgn}(w-c)\left|f_u(\boldsymbol{\gamma}, w)\right| \mathrm{d}w.$$

It is now possible to repeat the proofs of Lemmas 3–7 of [19], the only change being the contribution of the term $\lambda|\Delta_- h_{j+1/2}^n|$ appearing in (31).

2.3 *Numerical Examples (Examples 1 and 2)*

Consider a suspension characterized by $b(u) = v_{\mathrm{St}} u V(u)$, where $v_{\mathrm{St}} = 10^{-4}\,\mathrm{m/s}$ and $V(u)$ is given by (4) with $n_{\mathrm{RZ}} = 5$ and $u_{\max} = 1$. We assume that $A \equiv 0$ and consider a cylindrical CT with $x_{\mathrm{L}} = -1\,\mathrm{m}$ and $x_{\mathrm{R}} = 1\,\mathrm{m}$ with (nominal) interior cross-sectional area $S = 1\,\mathrm{m}^2$. The CT is assumed to initially contain no

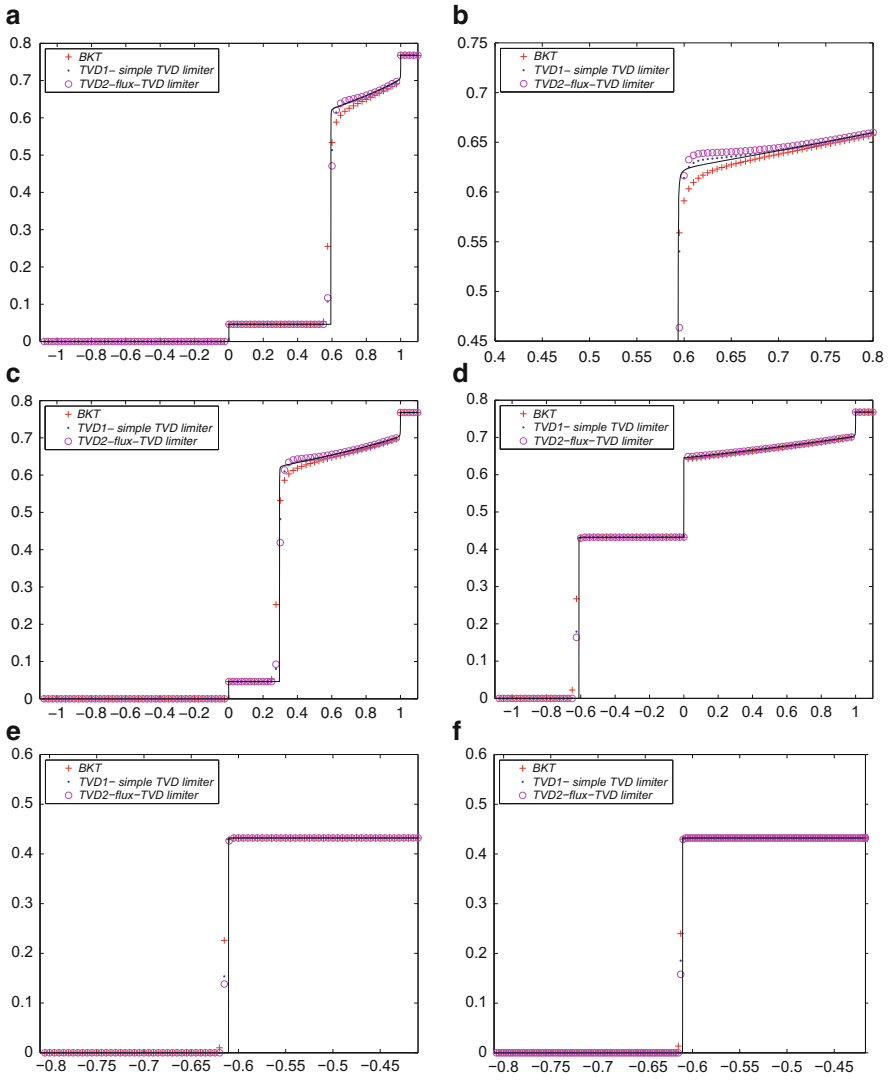

Fig. 3 Example 1: numerical solution at (**a**, **b**) $t = 150{,}000\,\mathrm{s}$ with (**a**) $J = 40$, (**b**) $J = 200$ (enlarged view around $x = 0.6$), at (**c**) $t = 250{,}000\,\mathrm{s}$ with $J = 40$, and at (**d**–**f**) $t = 500{,}000\,\mathrm{s}$ with (**d**) $J = 40$, (**e**) $J = 200$, (**f**) $J = 400$ ((**e**, **f**): enlarged view around $x = -0.61$). The *solid line* is the reference solution

solids ($u_0 \equiv 0$), is operated with a feed concentration $u_\mathrm{F} = 0.3$ in Example 1 and $u_\mathrm{F} = 0.5$ in Example 2, and the flow velocities are $q_\mathrm{L} = -1.0 \times 10^{-5}\,\mathrm{m/s}$ and $q_\mathrm{R} = 2.5 \times 10^{-6}\,\mathrm{m/s}$. In these examples, the solution is clearly not TVD, since $\mathrm{TV}(u_0) = 0$. Figure 3 shows the numerical solution for Example 1 calculated by the first-order scheme of [21] (BKT), the scheme described herein that uses the

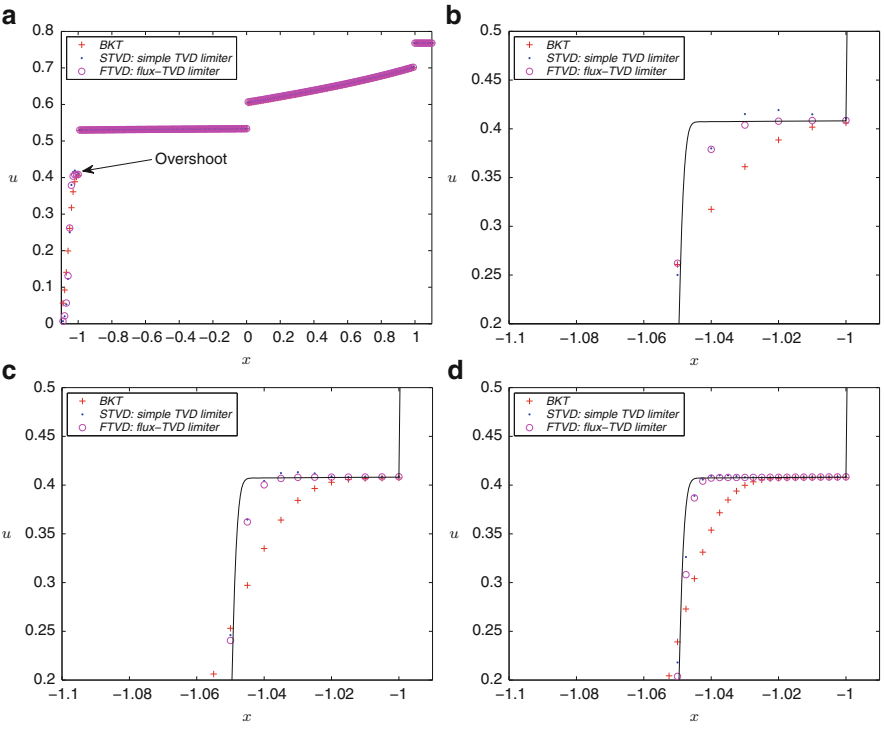

Fig. 4 Example 2: numerical solution at $t = 272{,}760$ s with (**a**, **b**) $J = 100$, (**c**) $J = 200$ and (**d**) $J = 400$ ((**b**–**d**): enlarged views around $x = -1$). The *solid line* is the reference solution

simple TVD (STVD) limiter (in short, STVD scheme), and the FTVD scheme. All calculations were performed with $\lambda = 2{,}000$ s/m, and results are compared against a reference solution calculated by the first-order scheme of [22] with $J = 100{,}00$, where $J = 1/\Delta x$ (in meters). Example 2 illustrates the overshoot mentioned in Sect. 2.2, see Fig. 4. We observe that Fig. 4 illustrates how the "overshoot" phenomenon diminishes as $\Delta x \to 0$.

The numerical solutions of Examples 1 and 2 indicate that the STVD and FTVD schemes are significantly more accurate than their first-order counterpart. It seems that both schemes STVD and FTVD, have comparable accuracy. A significant difference in solution behaviour between both schemes becomes visible in Fig. 4.

2.4 *A Note on Second-Order Degenerate Parabolic Equations (Example 3)*

The model (9) with a degenerate diffusion term can be handled by a Strang-type operator splitting scheme [85]. To describe it, let U^n denote the approximate

solution at time level n, and write the scheme (19) in operator notation via $U^{n+1} = \mathcal{H}(\Delta t)U^n$. Then the proposed operator splitting scheme for (9) is

$$U^{n+1} = \big[\mathcal{H}(\Delta t/2) \circ \mathcal{P}(\Delta t) \circ \mathcal{H}(\Delta t/2)\big]U^n, \quad n = 0, 1, 2, \ldots. \tag{32}$$

Here $\mathcal{P}(\Delta t)$ represents a second-order scheme for $u_t = (\gamma_1(x)A(u)_x)_x$ written as $U^{n+1} = \mathcal{P}(\Delta t)U^n$. If we employ the Crank-Nicolson (CN) scheme, which has second-order accuracy in space and time, then $\mathcal{P}(\Delta t)$ is defined by

$$U_j^{n+1} = U_j^n + \frac{\Delta t}{2\Delta x^2}\left[\Delta_+\left(s_{j-1/2}\Delta_- A_j^n\right) + \Delta_+\left(s_{j-1/2}\Delta_- A_j^{n+1}\right)\right]. \tag{33}$$

Here $s_{j-1/2}$ denotes our discretization of the parameter $\gamma_1(x)$. The CN scheme is stable with linear stability analysis. For our nonlinear problem, we generally need a very strong type of stability, both from a practical and theoretical point of view. It seems that it is impossible to get this type of strong stability for implicit schemes of accuracy greater than one [49]. On the other hand, the solution u is continuous in the regions where the parabolic operator is in effect (cf., e.g., [21]), which seems to stabilize the numerical approximation. The CN scheme leads to a nonlinear system of equations, which are solved here iteratively; each step of iteration requires solving a tridiagonal linear system (see [25]). These iterations have turned out to converge rather quickly.

Since each of the parabolic and hyperbolic operators has formal second-order accuracy in both space and time, we will maintain overall second order accuracy with the Strang splitting [85]. This is a well-known result, see, e.g., [48].

Next, we include the strongly degenerate diffusion term (10) with

$$a(u) = \frac{b(u)\sigma_e'(u)}{(\rho_s - \rho_f)gu},$$

where the so-called effective solid stress function $\sigma_e(u)$ is given by

$$\sigma_e(u) = \begin{cases} 0 & \text{for } u \le u_c, \\ \sigma_0\big((u/u_c)^k - 1\big) & \text{for } u > u_c, \end{cases}$$

where we use $\sigma_0 = 1\,\text{Pa}$, $u_c = 0.1$ and $k = 6$ along with $\Delta\rho = 1{,}500\,\text{kg/m}^3$ and $g = 9.81\,\text{m/s}^2$ [21]. The vessel and control variables are the same as in Example 1, and we again set $u_0 \equiv 0$. Figure 5 shows the numerical solution calculated by the semi-implicit scheme described in [21] (BKT-SI), the operator splitting scheme described herein (BKT-OS), the operator splitting scheme (32) and (33) including the simple TVD limiter (STVD-OS), and the analogue scheme involving the non-local limiter (FTVD-OS). All calculations were performed with $\lambda = 2{,}000\,\text{s/m}$.

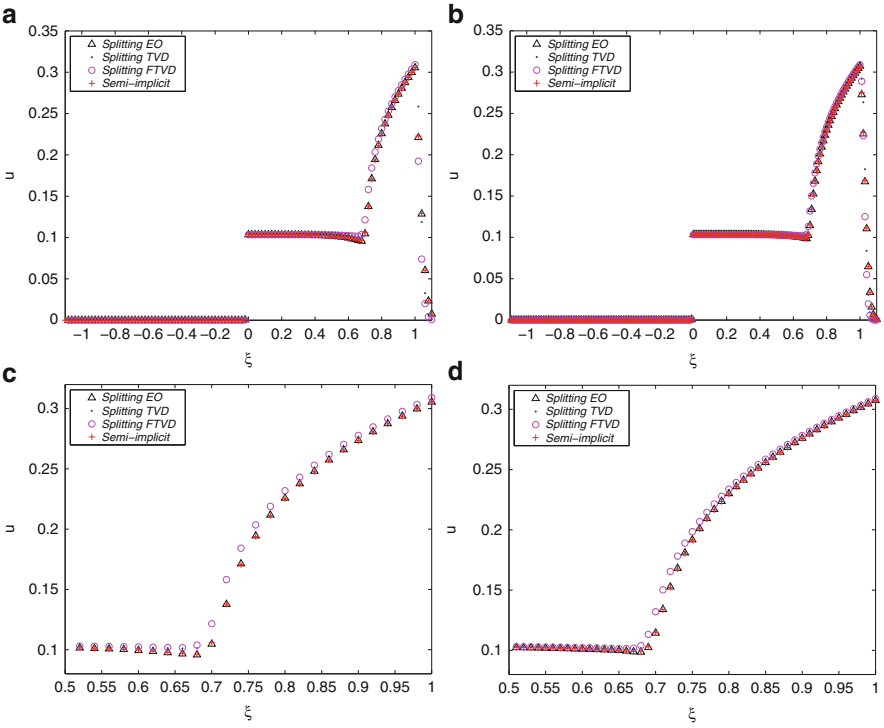

Fig. 5 Example 3: numerical solution at $t = 25{,}000\,\mathrm{s}$ with (**a**) $J = 50$, (**b**) $J = 100$, (**c**) at $t = 25{,}000\,\mathrm{s}$ with $J = 50$, (**d**) at $t = 100{,}000\,\mathrm{s}$ with $J = 50$

3 A Conservation Law with Nonlocal Flux Modeling Sedimentation

When diffusion is negligible, the one-dimensional continuity equation is (1), and the solids phase velocity v_s is given by (3) and (5). Assume now that V is given by (4) but depends on u in the nonlocal form

$$V = V(K_a * u), \quad (K_a * u)(x,t) = \int_{-2a}^{2a} K_a(y)u(x+y,t)\,\mathrm{d}y, \tag{34}$$

where K_a is a symmetric, non-negative piecewise smooth kernel with support on $[-2a, 2a]$ for a parameter $a > 0$ and $\int_{\mathbb{R}} K_a(x)\,\mathrm{d}x = 1$. Then (1) takes the form

$$u_t + v_{\mathrm{St}}\big(u(1 - K_a * u)^{n_{\mathrm{RZ}}}\big)_x = 0. \tag{35}$$

On the other hand, starting from the relation $v_s = (1-u)v_r$ valid for batch settling, we obtain the alternative governing equation $u_t + (u(1-u)v_r)_x = 0$.

If v_r (instead of v_s) has a nonlocal behaviour and the local versions based on specifying either v_s or v_r should coincide, then the constitutive assumption for v_r becomes $v_r = V(K_a * u)/(1-u)$. For instance, (4) leads to the conservation law

$$u_t + v_{St}\big(u(1-u)(1-K*u)^{n_{RZ}-1}\big)_x = 0. \tag{36}$$

Both (35) and (36) are special cases of (11).

3.1 Properties of the Nonlocal Equation

Insight into properties of (11) can be gained by analyzing an approximate local PDE (the "effective" local PDE [99]) obtained from the Taylor expansion of $K_a * u$. If $2M_2$ denotes the second moment of K_a, then we obtain the approximate diffusive-dispersive local PDE

$$u_t + \big(u(1-u)^\alpha V(u)\big)_x = -a^2 M_2 \big(V'(u)u(1-u)^\alpha u_{xx}\big)_x \tag{37}$$

(see [12] for details). For $\alpha \geq 1$ the factor $u(1-u)$ in the right-hand side and in the flux has a "saturating" effect; it prevents solution values from leaving $[0,1]$. Thus, we should expect that the nonlocal PDE (11) also satisfies an invariant region principle for $\alpha \geq 1$. This is indeed the case, as will be shown below.

We mention that Zumbrun [99] studied an equation equivalent to (11) in the case $\alpha = 0$ and $V(w) = v_{St}(1-\beta w)$, namely

$$u_t + \big(uK_a * u\big)_x = 0, \tag{38}$$

where $K_a(x) := a^{-1}K(a^{-1}x)$ and K is the truncated parabola given by

$$K(x) = \frac{3}{8}\left(1 - \frac{x^2}{4}\right) \text{ for } |x| < 2; \quad K(x) = 0 \text{ otherwise.} \tag{39}$$

He showed global existence of weak solutions for (12) and (38) in L^∞ and uniqueness in the class BV, and derived the effective local, dispersive, KdV-like PDE

$$u_t + (u^2)_x = -M_2 a^2 (uu_{xx})_x. \tag{40}$$

He showed by analyzing (40) that (38) supports travelling waves, but not viscous shocks. This result is based on the symmetry of K, which makes (38) completely dispersive. Moreover, an L^2 stability argument is invoked to conclude that smooth solutions of the Burgers-like first-order conservation law $u_t + (u^2)_x = 0$ arise from smooth solutions of (38) as $a \to 0$. Zumbrun [99] also studied the effect of artificial

diffusion added to (38), and showed that for the corresponding effective local PDE, solutions of shock initial data converge to a stable, oscillatory travelling wave.

For $\alpha = 0$, the notion of weak solution is sufficient for uniqueness and stability (at least in the Wasserstein distance, see [11, 66]), since the convolution introduces sufficient regularization to ensure that the advective velocity is Lipschitz continuous. This is true even with discontinuous data. For the case $\alpha = 0$, the analysis of [12] based on a quadrature-difference scheme comes to a corresponding Lipschitz continuity result for Lipschitz continuous initial data, as will be discussed below.

3.2 Numerical Scheme and Well-Posedness Analysis

We discretize (11) on a fixed grid given by $x_j = j\Delta x$ for $j \in \mathbb{Z}$ and $t_n = n\Delta t$ for $n \leq N := T/\Delta t$, where T is the finite final time. As usual, u_j^n approximates the cell average of $u(\cdot, t_n)$ on $(x_{j-1/2}, x_{j+1/2})$, and we define $U^n := (\ldots, u_{j-1}^n, u_j^n, u_{j+1}^n, \ldots)^{\mathrm{T}}$. The initial datum u_0 is discretized accordingly. We define the second spatial difference operator $\Delta^2 u_j^n := \Delta_+ \Delta_- u_j^n$.

We assume that K_a is a positive symmetric kernel, has compact support on $[-2a, 2a]$, $K_a \in C^{0,1}(\mathbb{R}) \cap C^2([-2a, 2a])$ and $\int_{-2a}^{2a} K_a(y)\,\mathrm{d}y = 1$. (The same analysis remains valid for more general kernels [12].) The integral in (34) is approximated by the quadrature formula

$$(K_a * u)_j^n \approx \tilde{u}_{a,j}^n := \sum_{i=-l}^{l} \gamma_i u_{j-i}^n, \text{ where } \gamma_i = \int_{x_i - 1/2}^{x_i + 1/2} K_a(y)\,\mathrm{d}y, \, l = \left\lceil \frac{2a}{\Delta x} \right\rceil + 1.$$

Due to the properties of K_a, $\gamma_{-l} + \cdots + \gamma_l = 1$. Furthermore, we require that u_0 has compact support, $u_0(x) \geq 0$ for $x \in \mathbb{R}$ and $u_0 \in BV(\mathbb{R})$. The function $u \mapsto V(u)$ and its derivatives are locally Lipschitz continuous for $u \geq 0$ (which occurs, for example, if $V(\cdot)$ is a polynomial). When we send $\Delta x, \Delta t \downarrow 0$ then it is understood that $\lambda := \Delta t/\Delta x$ is kept constant. Moreover, for the case $\alpha \geq 1$ we suppose that $u_0(x) \leq 1$ for all $x \in \mathbb{R}$.

From now on we let the function u^Δ be defined by

$$u^\Delta(x,t) = U_j^n \quad \text{for } (x,t) \in [j\Delta x, (j+1)\Delta x) \times [n\Delta t, (n+1)\Delta t).$$

Definition 2. A measurable, non-negative function u is an *entropy solution* of the initial value problem (11) and (12) if it satisfies the following conditions:

1. We have $u \in L^\infty(\Pi_T) \cap L^1(\Pi_T) \cap BV(\Pi_T)$.
2. The initial condition (12) is satisfied in the following sense:

$$\lim_{t \downarrow 0} \int_{\mathbb{R}} \left| u(x,t) - u_0(x) \right| \mathrm{d}x = 0.$$

3. For all non-negative test functions $\varphi \in C_0^\infty(\Pi_T)$, the following Kružkov-type [62] entropy inequality is satisfied, where we define $f(u) := u(1-u)^\alpha$:

$$\forall k \in \mathbb{R}: \quad \iint_{\Pi_T} \Big\{ |u-k|\varphi_t + \operatorname{sgn}(u-k)\big(f(u)-f(k)\big)V(K_a * u)\varphi_x - \operatorname{sgn}(u-k)\, f(k) V'(K_a * u)(\partial_x K_a * u)\varphi \Big\} \,\mathrm{d}x\,\mathrm{d}t \geq 0. \tag{41}$$

An entropy solution is, in particular, a weak solution of (11) and (12), which is defined by (1) and (2) of Definition 2, and the following equality, which must hold for all $\varphi \in C_0^\infty(\Pi_T)$:

$$\iint_{\Pi_T} \Big\{ u\,\varphi_t + f(u)V(K_a * u)\varphi_x - f(u)V'(K_a * u)(\partial_x K_a * u)\varphi \Big\} \,\mathrm{d}x\,\mathrm{d}t = 0.$$

Suitable Rankine-Hugoniot and entropy jump conditions can be derived from (41).

The uniqueness of entropy solutions follows from a result proved in [58] regarding continuous dependence of entropy solutions with respect to the flux function:

Theorem 2. *If u and v are entropy solutions of (11) and (12) with initial data u_0 and v_0, respectively, then for $T > 0$ there exists a constant C_1 such that*

$$\big\| u(\cdot,t) - v(\cdot,t) \big\|_{L^1(\mathbb{R})} \leq C_1 \, \|u_0 - v_0\|_{L^1(\mathbb{R})} \quad \forall t \in (0,T].$$

In particular, an entropy solution of (11) and (12) is unique.

Finally, let us briefly address the convergence analysis and the related result of existence of entropy solutions. To this end, let $V_j^n := V(\tilde{u}_{a,j}^n)$. Then the marching formula for the approximation of solutions of (11) and (12) reads

$$u_j^{n+1} = \frac{u_{j-1}^n + u_{j+1}^n}{2} - \frac{\lambda}{2} u_{j+1}^n \big(1-u_{j+1}^n\big)^\alpha V_{j+1}^n + \frac{\lambda}{2} u_{j-1}^n \big(1-u_{j-1}^n\big)^\alpha V_{j-1}^n. \tag{42}$$

We assume that $\lambda = \Delta t / \Delta x$ satisfies the following CFL condition:

$$\lambda \max_{u \leq u^*} \big|V(u)\big| < 1 \text{ for } \alpha = 0,\ u^* := \|K_a\|_\infty \|u_0\|_1;$$

$$\lambda \max_{0 \leq u \leq 1} \big|V(u)\big| < 1 \text{ for } \alpha \geq 1.$$

The convergence proof of the numerical scheme is based on the usual L^∞, BV and L^1 Lipschitz continuity in time bounds, where the latter two depend on T and adversely on a. The L^∞ bound is as follows:

$$0 \le u_j^n \le \begin{cases} C_3 & \text{if } \alpha = 0, \\ 1 & \text{if } \alpha \ge 1, \end{cases} \quad \text{for } j \in \mathbb{Z} \text{ and } 0 \le n \le N, \tag{43}$$

where the constant C_3 is independent of Δx and Δt but depends on T. This bound represents the most important estimate of the convergence analysis [12, Lemma 5.3]. In view of (37), one should expect an "invariant region" principle to hold for (11), (12) with $\alpha \ge 1$. The estimate (43) shows that this property indeed holds.

Invoking the bounds established so far and applying a Lax-Wendroff-type argument to the discrete entropy inequality

$$\left|u_j^{n+1} - k\right| - \left|u_j^n - k\right| + \mathcal{G}_{j+}^n - \mathcal{G}_{j-}^n + \operatorname{sgn}\left(u_j^{n+1} - k\right)\frac{\lambda}{2} f(k)\left(V_{j+1}^n - V_{j-1}^n\right) \le 0$$

satisfied by the scheme, where we define

$$\mathcal{G}_{j\pm}^n := \frac{\lambda}{2}\left[\left(f\left(u_{j\pm1}^n \vee k\right) - f\left(u_{j\pm1}^n \wedge k\right)\right) V_{j\pm1}^n - \frac{1}{\lambda}\Delta_\pm\left(\left|u_j^n - k\right|\right)\right],$$

we can conclude by Helly's theorem that u^Δ converges to a function $u \in L^\infty(\Pi_T) \cap L^1(\Pi_T) \cap BV(\Pi_T)$ as $\Delta x,\ \Delta t \to 0$, and prove the following theorem.

Theorem 3. *The numerical solution generated by* (42) *converges to the unique entropy solution of* (11) *and* (12).

As an additional regularity result for $\alpha = 0$, it can be shown that for $T > 0$, u^Δ converges to a Lipschitz continuous function u provided u_0 is also Lipschitz continuous. This result is as expected since in the simplest case, V constant, (11) becomes a linear advection equation, whose solution has a regularity that is the same as that of u_0. Moreover, as a Lipschitz continuous weak solution of (11) and (12), u will automatically be an entropy solution.

3.3 Numerical Examples

We illustrate in Example 4 how the value of a affects the numerical solution of (11) and (12) for $\alpha = 0$ and $\alpha = 1$. We use (4) with $n_{\mathrm{RZ}} = 5$ for $\alpha = 0$ and, correspondingly, (4) with $n_{\mathrm{RZ}} = 4$ for $\alpha = 1$. In both cases, K is given by (39) with $a = 0.4, 0.2, 0.1$, and 0.01. The initial datum is

$$u_0(x) = \begin{cases} 0.0 & \text{for } x \le 0.2, \\ 0.6 & \text{for } x > 0.2, \end{cases} \quad \text{and} \quad u_0(x) = \begin{cases} 0.0 & \text{for } x \le 0.2, \\ 0.01 & \text{for } x > 0.2, \end{cases}$$

for the two cases of a concentrated and a dilute suspension with $\Delta x = 0.0005$ and $\lambda = 0.2$. Figure 6 shows the numerical results. The case $a = 0.01$ was calculated

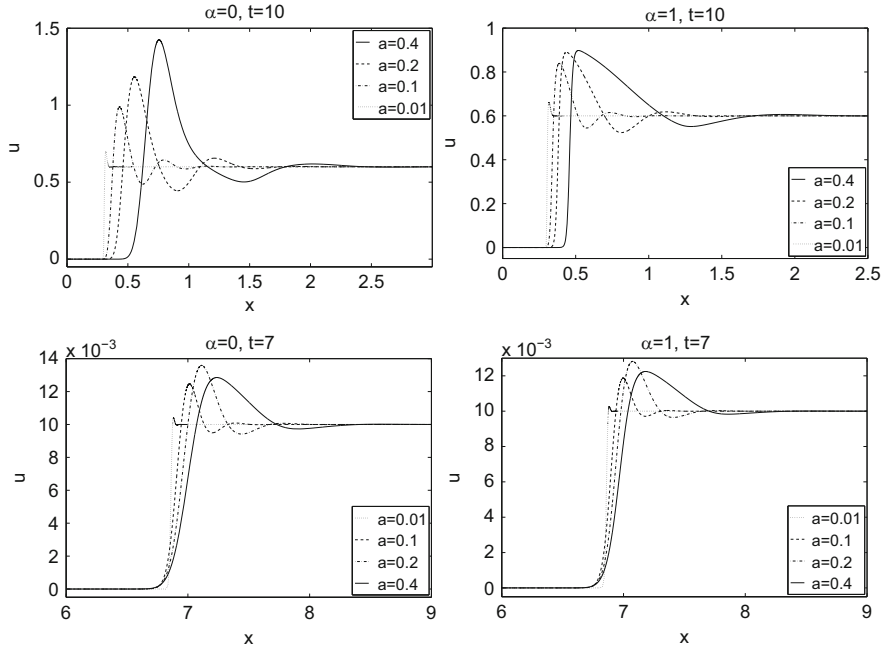

Fig. 6 Example 4: numerical solutions of (11) and (12) (*top*) for an initially concentrated suspension at $t = 10$ and (*bottom*) for an initially dilute suspension at $t = 7$

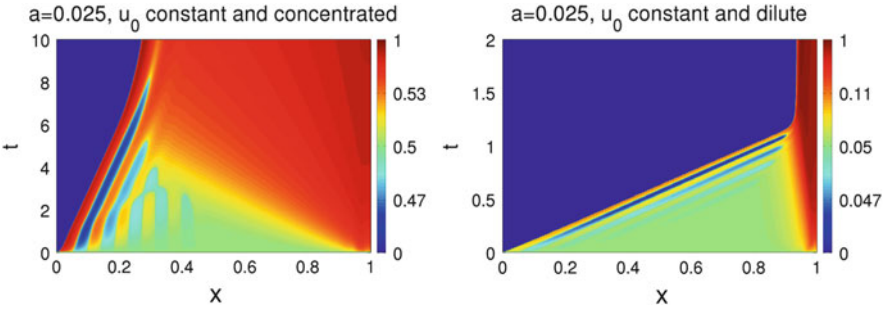

Fig. 7 Example 5: numerical solution of (11) and (12) with $\alpha = 1$ and initial data (44)

with $\Delta x = 0.0002$ since otherwise the stencil of the convolution includes just a few points. We observe a more strongly oscillatory behaviour with $a = 0.4$, 0.2 and 0.1 than with $a = 0.01$, and that the period of the oscillation is proportional to a.

In Example 5 we attempt to reproduce the layering phenomenon observed by Siano [81] for batch settling. In Fig. 7 we show the numerical results for $\alpha = 1$, with $V(u) = (1-u)^4$, K as in (39), $a = 0.025$, $\Delta x = 0.00025$, $\lambda = 0.5$ and the initial datum for the respective concentrated and dilute case

$$u_0(x) = \begin{cases} 0 & \text{for } x < 0, \\ 0.5 & \text{for } 0 \le x < 1, \\ 1 & \text{for } x \ge 1 \end{cases} \quad \text{and} \quad u_0(x) = \begin{cases} 0 & \text{for } x < 0, \\ 0.05 & \text{for } 0 \le x < 1, \\ 1 & \text{for } x \ge 1. \end{cases} \tag{44}$$

We observe layers of concentrations smaller or larger than the initial value u_0. These "stripes" are initially close to parallel to the supernate-suspension interface. However, stripes are obliterated as soon as interaction with concentration information travelling upwards from the vessel bottom takes place.

4 Kinematic Models of Polydisperse Sedimentation

Polydisperse sedimentation models belong to the wider class of multi-species kinematic flow models given by (13) with explicit velocity functions v_i, including the multi-class Lighthill-Whitham-Richards (MCLWR) kinematic traffic model [8,95]. The basic phenomenon of interest in these models, the segregation of species, is usually associated with the formation of discontinuities in Φ, so-called kinematic shocks. Other multi-species kinematic flow models also include the settling of oil-in-water dispersions [76] and of emulsions (cf., e.g., [22,47]).

For many multi-species kinematic flow models, the velocities v_i do not depend on each of the N components of Φ in an individual way, but are functions of $m \ll N$ ($m \le 4$ for all models of interest) scalar functions of Φ, i.e.,

$$v_i = v_i(p_1, \ldots, p_m), \quad p_l = p_l(\Phi), \quad l = 1, \ldots, m. \tag{45}$$

Thus, $\mathcal{J}_f(\Phi)$ is a rank-m perturbation of $\boldsymbol{D} := \operatorname{diag}(v_1, \ldots, v_N)$ of the form

$$\mathcal{J}_f = \boldsymbol{D} + \boldsymbol{B}\boldsymbol{A}^{\mathrm{T}}, \begin{cases} \boldsymbol{B} := (B_{il}) = (\phi_i \partial v_i / \partial p_l), \\ \boldsymbol{A} := (A_{jl}) = (\partial p_l / \partial \phi_j), \end{cases} \quad 1 \le i, j \le N,\ 1 \le l \le m. \tag{46}$$

The analysis in [24] also provides sharp bounds of the eigenvalues of $\mathcal{J}_f(\Phi)$. This information permits to numerically calculate the eigenvalues and corresponding eigenvectors of $\mathcal{J}_f(\Phi)$ with acceptable effort. This characteristic (or spectral) information can be exploited for the implementation of high-resolution schemes.

High-resolution shock capturing schemes can be applied to systems of conservation laws either in a component-wise or in a characteristic-wise (spectral) fashion. The latter requires a detailed knowledge of the spectral decomposition of the Jacobian matrix of the system. For multi-species kinematic flow models, however, eigenvalues are not available in closed form. Nevertheless, it has been possible to prove strict hyperbolicity of some of these models by an explicit representation of the characteristic polynomial [10,76,97], as well as to obtain an interlacing property

of the (unknown) eigenvalues λ_i of the Jacobian with the (known) velocities v_i, which provide excellent starting values for a root finder. For the MCLWR model, these results can be found in [97, 98] and in references cited in these papers.

Donat and Mulet [43] showed that the hyperbolicity calculus of multi-species kinematic flow models satisfying (45) can be greatly simplified by using the so-called secular equation [1], which provides a systematic algebraic framework to determine the eigenvalues, and eventually the eigenvectors, but avoids the explicit representation of the characteristic polynomial. The hyperbolicity analysis for the MCLWR model becomes very simple. Via the secular approach, hyperbolicity of the MLB model for equal-density spheres (a case of $m = 2$) can be proved in a few lines [43], which contrasts with several pages of computation necessary to exhibit the characteristic polynomial in [10]. In [24] the secular approach was used to estimate the region of hyperbolicity of the HS model, for which $m = 3$ or $m = 4$. In [26] the results of [24] are employed to implement characteristic-wise WENO schemes for the polydisperse sedimentation model. On the other hand, there are also other polydisperse sedimentation models (besides the MLB and HS models) for which the flux Jacobian is a rank-m perturbation of a diagonal, and to which a version of the present numerical technique can be applied [27, 38, 72].

4.1 Hyperbolicity Analysis

The hyperbolicity analysis of (13) under the assumption (45) is then based on the following theorem.

Theorem 4 (The secular equation, [1, 43]). *Assume that $v_i > v_j$ for $i < j$, and that $\boldsymbol{A}$ and $\boldsymbol{B}$ have the formats specified in (46). We denote by S_r^p the set of all (ordered) subsets of r elements taken from a set of p elements. If $\boldsymbol{X}$ is an $m \times N$ matrix, $I := \{i_1 < \cdots < i_k\} \in S_k^N$ and $J := \{j_1 < \cdots < j_l\} \in S_l^m$, then we denote by $\boldsymbol{X}^{I,J}$ the $k \times l$ submatrix of $\boldsymbol{X}$ given by $(\boldsymbol{X}^{I,J})_{p,q} = X_{i_p,j_q}$. Let $\lambda \neq v_i$ for $i = 1, \ldots, N$. Then λ is an eigenvalue of $\boldsymbol{D} + \boldsymbol{B}\boldsymbol{A}^{\mathrm{T}}$ if and only if*

$$R(\lambda) := \det\bigl(\boldsymbol{I} + \boldsymbol{A}^{\mathrm{T}}(\boldsymbol{D} - \lambda \boldsymbol{I})^{-1}\boldsymbol{B}\bigr) = 1 + \sum_{i=1}^{N} \frac{\gamma_i}{v_i - \lambda} = 0, \tag{47}$$

$$\text{where} \quad \gamma_i := \sum_{r=1}^{\min\{N,m\}} \sum_{I \in S_r^N, J \in S_r^m} \frac{\det \boldsymbol{A}^{I,J} \det \boldsymbol{B}^{I,J}}{\prod_{l \in I, l \neq i}(v_l - v_i)}.$$

The relation $R(\lambda) = 0$, (47), is known as the secular equation *[1].*

Assuming that $m < N$, with $\boldsymbol{A}$ and $\boldsymbol{B}$ defined in (46) we can write

$$\gamma_i = \phi_i \sum_{r=1}^{m} \gamma_{r,i}, \quad \gamma_{r,i} = \sum_{i \in I \in S_r^N} \prod_{l \in I, l \neq i} \frac{\phi_l}{v_l - v_i} \sum_{J \in S_r^m} \det\left(\frac{\partial v_I}{\partial p_J}\right) \det\left(\frac{\partial p_J}{\partial \phi_I}\right).$$

When $m \leq 2$, these quantities can be easily computed and the hyperbolicity analysis via Theorem 4 is much less involved than explicitly deriving and discussing $\det(\mathcal{J}_f(\Phi) - \lambda \boldsymbol{I})$. For $m = 3$ or $m = 4$, the computations are more involved [24,27], but provide at least partial results concerning hyperbolicity, where the theoretical analysis of $\det(\mathcal{J}_f(\Phi) - \lambda \boldsymbol{I})$ is essentially out of reach.

The following corollary follows from Theorem 4 by a discussion of the poles of $R(\lambda)$ and its asymptotic behaviour as $\lambda \to \pm\infty$.

Corollary 1 ([24]). *If $\gamma_i \cdot \gamma_j > 0$ for $i, j = 1, \ldots, N$, then $\boldsymbol{D} + \boldsymbol{B}\boldsymbol{A}^{\mathrm{T}}$ is diagonalizable with real eigenvalues λ_i. If $\gamma_1, \ldots, \gamma_N < 0$, then the* interlacing property

$$M_1 := v_N + \gamma_1 + \cdots + \gamma_N < \lambda_N < v_N < \lambda_{N-1} < \cdots < \lambda_1 < v_1$$

holds, while for $\gamma_1, \ldots, \gamma_N > 0$, the following analogous property holds:

$$v_N < \lambda_N < v_{N-1} < \lambda_{N-1} < \cdots < v_1 < \lambda_1 < M_2 := v_1 + \gamma_1 + \cdots + \gamma_N.$$

The analysis of (47) also leads to an explicit spectral decomposition of $\mathcal{J}_f$ required for spectral schemes. Assume λ is an eigenvalue of $\mathcal{J}_f$ that satisfies $\lambda \neq v_i$ for all $i = 1, \ldots, N$. Then $\boldsymbol{\xi} = \boldsymbol{A}^{\mathrm{T}}\boldsymbol{x}$ is a solution of $\boldsymbol{M}_\lambda \boldsymbol{\xi} = \boldsymbol{0}$, where the $m \times m$ matrix $\boldsymbol{M}_\lambda := \boldsymbol{I} + \boldsymbol{A}^{\mathrm{T}}(\boldsymbol{D} - \lambda \boldsymbol{I})^{-1}\boldsymbol{B}$ can easily be computed. In fact, given $\boldsymbol{g}, \boldsymbol{h} \in \mathbb{R}^N$, if we use the notation

$$[\boldsymbol{g}, \boldsymbol{h}] := [\boldsymbol{g}, \boldsymbol{h}]_\lambda := \boldsymbol{g}^{\mathrm{T}}(\boldsymbol{D} - \lambda \boldsymbol{I})^{-1}\boldsymbol{h} = \sum_{k=1}^{N} \frac{g_k h_k}{v_k - \lambda},$$

then $\boldsymbol{M}_\lambda = \boldsymbol{I} + ([\boldsymbol{a}_i, \boldsymbol{b}_j])_{1 \leq i,j \leq m}$, where $\boldsymbol{a}_i$ and $\boldsymbol{b}_j$ are the columns of $\boldsymbol{A}$ and $\boldsymbol{B}$, respectively. If $\boldsymbol{\xi} \neq \boldsymbol{0}$ solves $\boldsymbol{M}_\lambda \boldsymbol{\xi} = \boldsymbol{0}$, then we can use $\boldsymbol{x} + (\boldsymbol{D} - \lambda \boldsymbol{I})^{-1}\boldsymbol{B}(\boldsymbol{A}^{\mathrm{T}}\boldsymbol{x}) = \boldsymbol{0}$ to compute a right eigenvector of $\mathcal{J}_f$ as $\boldsymbol{x} = -(\boldsymbol{D} - \lambda \boldsymbol{I})^{-1}\boldsymbol{B}\boldsymbol{\xi}$. The same procedure may be employed to calculate the left eigenvectors of $\mathcal{J}_f$.

The MLB model arises from the mass and linear momentum balance equations for the solid species and the fluid [10]. For equal-density particles, its final form is

$$v_i(\Phi) = v_i^{\mathrm{MLB}}(\Phi) := \frac{(\rho_{\mathrm{s}} - \rho_{\mathrm{f}})gD_1^2}{18\mu_{\mathrm{f}}}(1 - \phi)\mathcal{V}(\phi)\left(d_i^2 - \sum_{m=1}^{N} \phi_m d_m^2\right),$$

where μ_{f} is the fluid viscosity, and $\phi = \phi_1 + \cdots + \phi_N$ is the total solids volume fraction. Here $\mathcal{V}(\phi)$ is assumed to satisfy $\mathcal{V}(0) = 1$, $\mathcal{V}(\phi_{\max}) = 0$ and $\mathcal{V}'(\phi) \leq 0$

for $\phi \in [0, \phi_{\max}]$, where the maximum total solids concentration is assumed to be given by the constant $\phi_{\max}$. A standard choice for $\mathcal{V}(\phi)$ is the equation

$$\mathcal{V}(\phi) = \begin{cases} (1-\phi)^{n_{\mathrm{RZ}}-2} & \text{if } \Phi \in \mathcal{D}_{\phi_{\max}} \\ 0 & \text{otherwise,} \end{cases} \qquad n_{\mathrm{RZ}} > 2. \tag{48}$$

(This formula is consistent with (4) for $N = 1$, i.e., $V(\phi) = (1-\phi)^2\mathcal{V}(\phi)$.) We may write the components of the flux vector $\boldsymbol{f}(\Phi)$ of the MLB model as

$$f_i(\Phi) = f_i^{\mathrm{MLB}}(\Phi) := v_1^{\mathrm{MLB}}(\mathbf{0})\phi_i(1-\phi)\mathcal{V}(\phi)\left(d_i^2 - \sum_{m=1}^{N}\phi_m d_m^2\right). \tag{49}$$

The present version of the MLB model corresponds to $m = 2$, where $p_1 = \phi$ and $p_2 = \mathcal{V}(\phi)(d_1^2\phi_1 + \cdots + d_N^2\phi_N)$. For this model, we have:

Lemma 2 ([24]). *The MLB model (13) and (49) is strictly hyperbolic on $\mathcal{D}_{\phi_{\max}}$. The eigenvalues $\lambda_i = \lambda_i(\Phi)$ of $\mathcal{J}_f(\Phi) = \mathcal{J}_{\boldsymbol{f}^{\mathrm{MLB}}}(\Phi)$ satisfy the interlacing property*

$$M_1(\Phi) < \lambda_N(\Phi) < v_N(\Phi) < \lambda_{N-1}(\Phi) < v_{N-1}(\Phi) < \cdots < \lambda_1(\Phi) < v_1(\Phi), \tag{50}$$

$$M_1(\Phi) := v_1^{\mathrm{MLB}}(\mathbf{0})\left(d_N^2 V(\Phi) + \big((1-\phi)V'(\phi) - 2V(\phi)\big)\sum_{m=1}^{N}\phi_m d_m^2\right).$$

Furthermore, if $\lambda \notin \{v_1, \ldots, v_N\}$ is an eigenvalue of $\mathcal{J}_f(\Phi)$, then the discussion following Corollary 1 allows us to express the corresponding eigenvector in closed algebraic form (not detailed here).

The Höfler and Schwarzer (HS) model is motivated by the following expression for v_i by Batchelor and Wen [5,7], valid for a dilute suspension (i.e., $\phi \ll \phi_{\max}$):

$$v_i(\Phi) = \frac{(\rho_{\mathrm{s}} - \rho_{\mathrm{f}})gD_1^2}{18\mu_{\mathrm{f}}}d_i^2(1 + \boldsymbol{s}_i^{\mathrm{T}}\Phi). \tag{51}$$

Here, $\boldsymbol{s}_i^{\mathrm{T}} := (S_{i1}, \ldots, S_{iN})$ is the i-th row of the matrix $\boldsymbol{S} = (S_{ij})_{1\le i,j\le N}$ of dimensionless sedimentation coefficients S_{ij}, which are negative functions of $\lambda_{ij} := d_j/d_i$ and depend on certain other parameters. They can be reasonably approximated by

$$S_{ij} = \sum_{l=0}^{3}\beta_l\left(\frac{d_j}{d_i}\right)^l, \quad 1 \le i, j \le N \quad \text{with coefficients } \beta_0, \ldots, \beta_3 \le 0. \tag{52}$$

Some authors set $\beta_3 = 0$ a priori; for example, Höfler and Schwarzer [56] obtained

$$\boldsymbol{\beta}^{\mathrm{T}} = (\beta_0, \ldots, \beta_3) = (-3.52, -1.04, -1.03, 0) \tag{53}$$

by fitting data from [7] to a second-order polynomial. For simplicity, we also consider $\beta_3 = 0$ in this work.

To overcome the limitation of (51) to dilute suspensions, Höfler and Schwarzer [56] extended (51) to the whole range of concentrations by the formula

$$v_i(\Phi) = v_i^{\mathrm{HS}}(\Phi) := \frac{(\rho_{\mathrm{s}} - \rho_{\mathrm{f}})gD_1^2}{18\mu_{\mathrm{f}}} d_i^2 \exp(\boldsymbol{s}_i^{\mathrm{T}}\Phi + n\phi)(1-\phi)^n, \quad n \geq 0.$$

The corresponding flux vector of the HS model is given by

$$f_i(\Phi) = f_i^{\mathrm{HS}}(\Phi) := v_1^{\mathrm{HS}}(\mathbf{0})\phi_i d_i^2 \exp(\boldsymbol{s}_i^{\mathrm{T}}\Phi + n\phi)(1-\phi)^n.$$

For the HS model it is straightforward to verify strict hyperbolicity on $\mathcal{D}_1$ for $N = 2$, arbitrary non-positive Batchelor matrices $\boldsymbol{S}$ and arbitrarily small values of d_2. The analysis of [24] ensures hyperbolicity for arbitrary N and in the case of the coefficients (53) under the fairly mild restriction $d_N > 0.0078595$.

For the hyperbolicity analysis of the HS model, we define

$$\boldsymbol{a}_\nu := \boldsymbol{d}_{\nu-1}^{\mathrm{T}} := \left(d_1^{\nu-1}, d_2^{\nu-1}, \ldots, d_N^{\nu-1}\right), \quad p_\nu := \boldsymbol{a}_\nu^{\mathrm{T}}\Phi, \quad \nu = 1, \ldots, 4,$$

and taking into account that $\beta_3 = 0$, we obtain from (51) and (52)

$$v_i(\Phi) = v_1^{\mathrm{HS}}(\mathbf{0}) d_i^2 \exp\left((\beta_0 + n)p_1 + \frac{\beta_1}{d_i}p_2 + \frac{\beta_2}{d_i^2}p_3\right)(1-p_1)^n.$$

Thus, the hyperbolicity of the HS model can be analyzed by Theorem 4, where $m = 3$ if $\beta_3 = 0$ and $m = 4$ if $\beta_3 \neq 0$. The calculations become involved, but still lead to estimates of the hyperbolicity region. A typical result is the following.

Lemma 3. *Assume that $\boldsymbol{\beta}$, $\phi_{\max}$, and the width of the particle size distribution characterized by the value of $d_N \in (0, 1]$ satisfy*

$$H(\phi, \boldsymbol{\beta}, d_N) := -\tilde{\beta}_0\left(\beta_1 d_N + \beta_2(1+d_N)^2\right) - \beta_2\beta_1 d_N - \phi(1-d_N)^2\tilde{\beta}_0\beta_1\beta_2 < 0$$

for all $\phi \in (0, \phi_{\max})$. Then the HS model is strictly hyperbolic for $\Phi \in \mathcal{D}_{\phi_{\max}}$. The eigenvalues satisfy the interlacing property (50). (The fairly involved algebraic expression for γ_i for this model is not written out here for brevity. We refer to [24] and [27] for the respective cases $\beta_3 = 0$ and $\beta_3 < 0$.)

For $\boldsymbol{\beta}$ given by (53) the region of hyperbolicity for the HS model ensured by Lemma 3 is illustrated in Fig. 8. The spectral decomposition of $\mathcal{J}_{\boldsymbol{f}}(\Phi)$, i.e., the eigenvectors corresponding to the eigenvalues $\lambda_i(\Phi)$, is easy to obtain from Theorem 4, see [26] for details. Similar estimates of the hyperbolicity region for

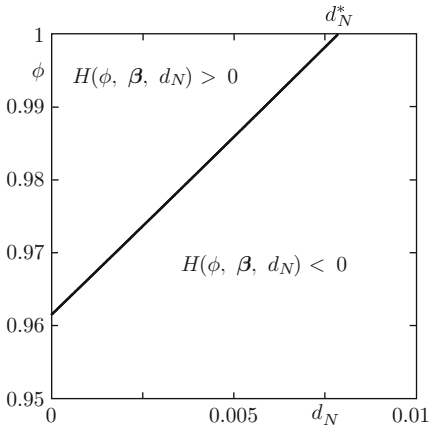

Fig. 8 Region of hyperbolicity ($H(\phi, \boldsymbol{\beta}, d_N) < 0$) for the HS model for the coefficients (53) [24]

the original model by Batchelor and Wen [5, 7], which is not discussed in this contribution, and for the HS model can be obtained by the same method for the case $\beta_3 < 0$, which gives rise to a perturbation rank of $m = 4$ [27].

4.2 Spectral and Component-Wise Numerical Schemes

For grid points $x_j = j\Delta x$, $t_n = n\Delta t$, a conservative scheme for $\Phi_i^n \approx \Phi(x_j, t_n)$ is given by

$$\Phi_j^{n+1} = \Phi_j^n - \frac{\Delta t}{\Delta x}\left(\hat{\boldsymbol{f}}_{j+1/2} - \hat{\boldsymbol{f}}_{j-1/2}\right), \quad \hat{\boldsymbol{f}}_{j+1/2} = \hat{\boldsymbol{f}}\left(\Phi_{j-s+1}^n, \ldots, \Phi_{j+s}^n\right), \quad j \in \mathbb{Z}.$$

The resulting scheme should be (at least second-order) accurate and stable. The most common design of numerical fluxes $\hat{\boldsymbol{f}}_{j+1/2}$ is to solve Riemann problems, either exactly (as in the original Godunov scheme, which is very costly), or approximately (e.g., as in the Roe scheme). For polydisperse sedimentation, exact Riemann solvers are out of reach, since the eigenstructure of $\mathcal{J}_{\boldsymbol{f}}$ is hard to compute.

In [26] Shu-Osher's technique [80] is used along with the information provided by the secular equation to get efficient schemes for the MLB and HS models. This scheme is based on the method of lines, that is, on applying an ODE solver to spatially semi-discretized equations. For the discretization of the flux derivative we use local characteristic projections. Local characteristic information to compute $\hat{\boldsymbol{f}}_{j+1/2}$ is provided by the eigenstructure of $\mathcal{J}_{\boldsymbol{f}}(\Phi_{j+1/2})$, where $\Phi_{j+1/2} = \frac{1}{2}(\Phi_j + \Phi_{j+1})$, given by the right and left eigenvectors that form the respective matrices

$$\boldsymbol{R}_{j+1/2} = \left[\boldsymbol{r}_{j+1/2,1} \ \ldots \ \boldsymbol{r}_{j+1/2,N}\right], \quad \left(\boldsymbol{R}_{j+1/2}^{-1}\right)^{\mathrm{T}} = \left[\boldsymbol{l}_{j+1/2,1} \ \ldots \ \boldsymbol{l}_{j+1/2,N}\right].$$

From a local flux-splitting $\boldsymbol{f}^{\pm,k}$ (we omit its dependency on $j+1/2$) given by $\boldsymbol{f}^{-,k}+\boldsymbol{f}^{+,k}=\boldsymbol{f}$, where $\pm\lambda_k(\mathcal{J}_{\boldsymbol{f}^{\pm,k}}(\Phi))\geq 0$, $\Phi\approx\Phi_{i+1/2}$ and λ_k is the k-th eigenvalue, $k=1,\ldots,N$, we can define the k-th characteristic flux as

$$g_j^{\pm,k}=\boldsymbol{l}_{j+1/2,k}^{\mathrm{T}}\cdot\boldsymbol{f}^{\pm,k}(\Phi_j).$$

If $\mathcal{R}^+$ and $\mathcal{R}^-$ denote upwind-based reconstructions, then

$$\hat{g}_{j+1/2,k}=\mathcal{R}^+\big(g_{j-s+1}^{+,k},\ldots,g_{j+s-1}^{+,k};x_{j+1/2}\big)+\mathcal{R}^-\big(g_{j-s+2}^{-,k},\ldots,g_{j+s}^{-,k};x_{j+1/2}\big),$$

$$\hat{\boldsymbol{f}}_{j+1/2}=\boldsymbol{R}_{j+1/2}\hat{\boldsymbol{g}}_{j+1/2}=\sum_{k=1}^{n}\hat{g}_{j+1/2,k}\boldsymbol{r}_{j+1/2,k}.$$

If we do not want to use local characteristic information, we can use the previous formula with $\boldsymbol{R}_{j+1/2}=\boldsymbol{I}_N$, where $\boldsymbol{I}_N$ denotes the $N\times N$ identity matrix, and a global flux splitting $\boldsymbol{f}^-+\boldsymbol{f}^+=\boldsymbol{f}$, where $\pm\lambda_k(\mathcal{J}_{\boldsymbol{f}^\pm}(\Phi)')\geq 0$ for all k. With this choice, and denoting by $\boldsymbol{e}_k$ the kth unit vector, we get $g_j^{\pm,k}=\boldsymbol{e}_k^{\mathrm{T}}\boldsymbol{f}^{\pm}(\Phi_j)=f_k^{\pm}(\Phi_j)$, i.e., $g_j^{\pm,k}$ are the components of the split fluxes, and the numerical flux is computed component by component by reconstructing the split fluxes component by component, i.e., $\hat{\boldsymbol{f}}_{j+1/2}=(\hat{f}_{j+1/2,1},\ldots,\hat{f}_{j+1/2,N})^{\mathrm{T}}$, where

$$\begin{aligned}\hat{f}_{j+1/2,k}=&\,\mathcal{R}^+\big(g_{j-s+1}^{+,k},\ldots,g_{j+s-1}^{+,k};x_{j+1/2}\big)\\&+\mathcal{R}^-\big(g_{j-s+2}^{-,k},\ldots,g_{j+s}^{-,k};x_{j+1/2}\big),\quad k=1,\ldots,N.\end{aligned}$$

This scheme will be referred to as COMP-GLF and it is a high-order extension of the Lax-Friedrichs scheme.

We now explain the SPEC-INT scheme. If $\lambda_k(\mathcal{J}_{\boldsymbol{f}}(\Phi))>0$ (respectively, <0) for all $\Phi\in[\Phi_j,\Phi_{j+1}]$, where $[\Phi_j,\Phi_{j+1}]\subset\mathbb{R}^N$ denotes the segment joining both states, then we upwind (since then there is no need for flux splitting):

$$\boldsymbol{f}^{+,k}=\boldsymbol{f},\ \boldsymbol{f}^{-,k}=\boldsymbol{0}\quad\text{if }\lambda_k(\mathcal{J}_{\boldsymbol{f}}(\Phi))>0,\quad \boldsymbol{f}^{+,k}=\boldsymbol{0},\ \boldsymbol{f}^{-,k}=\boldsymbol{f}\quad\text{if }\lambda_k(\mathcal{J}_{\boldsymbol{f}}(\Phi))<0.$$

On the other hand, if $\lambda_k(\mathcal{J}_{\boldsymbol{f}}(\Phi))$ changes sign on $[\Phi_j,\Phi_{j+1}]$, then we use a Local Lax-Friedrichs flux splitting given by $\boldsymbol{f}^{\pm,k}(\Phi)=\boldsymbol{f}(\Phi)\pm\alpha_k\Phi$, where the numerical viscosity parameter α_k should satisfy

$$\alpha_k\geq\max_{\Phi\in[\Phi_j,\Phi_{j+1}]}\big|\lambda_k\big(\mathcal{J}_{\boldsymbol{f}}(\Phi)\big)\big|.\tag{54}$$

The following usual choice of α_k produces oscillations in the numerical solution indicating that the amount of numerical viscosity is insufficient:

$$\alpha_k=\max\big\{\big|\lambda_k\big(\mathcal{J}_{\boldsymbol{f}}(\Phi_j)\big)\big|,\big|\lambda_k\big(\mathcal{J}_{\boldsymbol{f}}(\Phi_{j+1})\big)\big|\big\}.$$

The right-hand side of (54) can usually cannot be evaluated exactly in closed form. However, for the present class of models, Corollary 1 generates a fairly sharp bound for that expression. In the case of the MLB model, we have $\gamma_k < 0$ and the interlacing property leads to the efficiently computable bounds [26]

$$\max_{\Phi\in[\Phi_j,\Phi_{j+1}]} |\lambda_k(\Phi)| \le \alpha_k := \max\left\{ \max_{\Phi\in[\Phi_j,\Phi_{j+1}]} \left|v_k(\Phi)\right|, \max_{\Phi\in[\Phi_j,\Phi_{j+1}]} \left|v_{k+1}(\Phi)\right| \right\}, \quad k = 1,\ldots,N. \tag{55}$$

(This property also holds for other models, under appropriate circumstances [24, 27].) "SPEC-INT" denotes the scheme for which $\alpha_1,\ldots,\alpha_N$ are defined by (55).

4.3 Numerical Examples

The zero-flux boundary conditions (14) are implemented by setting $\hat{\boldsymbol{f}}_{-1/2} = \hat{\boldsymbol{f}}_{M-1/2} = 0$. We recall that a WENO5 scheme requires the consideration of two additional ghost cells on each boundary of the computational domain. To guarantee that all the interpolatory stencils remain inside the computational domain we set large values for the concentrations in the ghost cells, which produce large variations, so that the WENO procedure avoids the use of any stencil involving the ghost cells. The time discretization employs the well-known optimal third-order, three-stage Runge-Kutta method named SSPRK(3,3). SSP time discretization methods are widely used for hyperbolic PDE because they preserve the nonlinear stability properties which are necessary for problems with non-smooth solutions. To satisfy the CFL condition, the value of Δt is computed adaptively for each step ν. More precisely, the solution $\boldsymbol{\Phi}^{\nu+1}$ at $t_{\nu+1} = t_\nu + \Delta t$ is calculated from $\boldsymbol{\Phi}^\nu$ by using the time step $\Delta t = \mathrm{CFL} * \Delta x/\rho^\nu_{\max}$, where $\rho^\nu_{\max}$ is an estimate of the maximal characteristic velocity for $\boldsymbol{\Phi}^\nu$.

From [26] we select the case $N = 4$ for the MLB and HS models (Examples 6 and 7, respectively). We consider $d_1 = 1$, $d_2 = 0.8$, $d_3 = 0.6$ and $d_4 = 0.4$, $\phi_{\max} = 0.6$, and $\phi_i^0 = 0.05$ for $i = 1,\ldots,4$. We furthermore choose $D_1 = 4.96 \times 10^{-4}$ m, a settling vessel of (unnormalized) depth $L = 0.3$ m and $\phi_{\max} = 0.68$. We employ (48) with $n_{\mathrm{RZ}} = 4.7$. The remaining parameters are $g = 9.81\,\mathrm{m/s^2}$, $\mu_{\mathrm{f}} = 0.02416\,\mathrm{Pa\,s}$ and $\rho_{\mathrm{f}} = 1{,}208\,\mathrm{kg/m^3}$. Moreover, the spatial coordinate $x \in [0,1]$ refers to normalized depth. In this section, we take CFL = 0.5 throughout.

Figures 9a and 10a display the reference solution obtained with SPEC-INT and $M_{\mathrm{ref}} = 6{,}400$ for $t = 50$ s and $t = 300$ s respectively, while plots (b–d) of both figures are enlarged views of the corresponding numerical solutions obtained with SPEC-INT and COMP-GLF with $M = 400$. Figure 11 shows the corresponding results for Example 7. Both series of plots show that at $M = 400$ the quality of approximation of piecewise constant portions of the solution and the resolution of kinematic shocks by SPEC-INT is superior to that of COMP-GLF. For the times

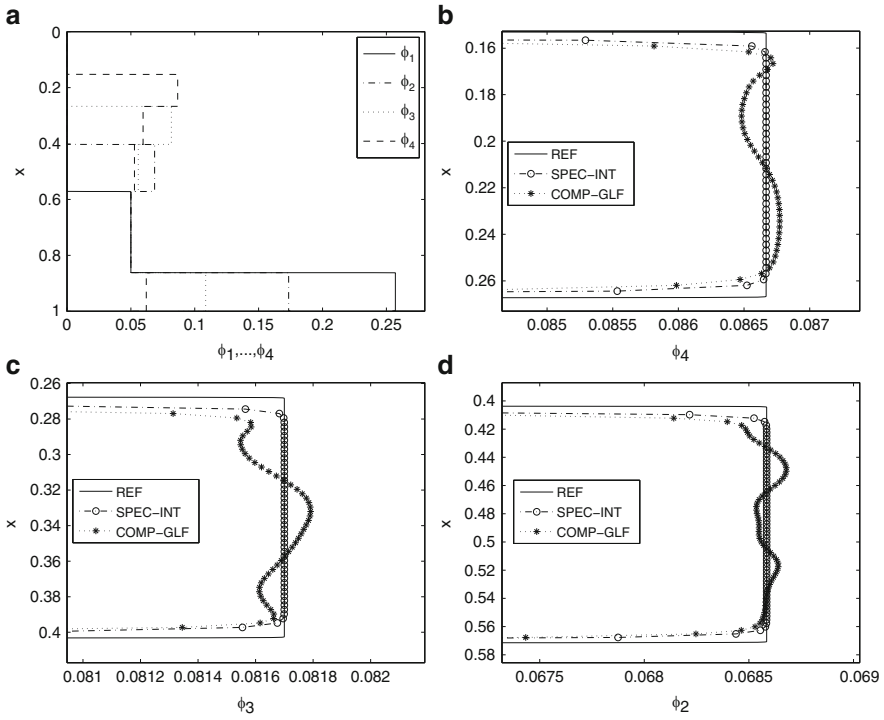

Fig. 9 Example 6: reference solution for $\phi_1, \ldots, \phi_4$ computed by SPEC-INT with $M_{\text{ref}} = 6{,}400$ (**a**), and details of numerical solutions with $M = 400$ (**b**–**d**) at $t = 50$ s

considered the average convergence rate using SPEC-INT is close to one. On the other hand, as time increases, the errors increase considerably. Of course, for a given value of M, COMP-GLF is faster than SPEC-INT. Nevertheless, if we seek a fixed level of resolution in the numerical simulation, then SPEC-INT turns out to be computationally more efficient, see [26].

As in the case of the MCLWR kinematic traffic models, the characteristic-based schemes, which use the full spectral decomposition of $\mathcal{J}_f$ at each cell-interface, are more robust and lead to numerical solutions which are essentially oscillation free. This situation is similar to what is observed for the Euler equations for gas dynamics, where the superiority of characteristic-based schemes is well known. For gas dynamics, the spectral decomposition of the Jacobian matrix is given in closed form, hence characteristic-based schemes pose no special difficulties. For polydisperse models, the spectral decomposition can only be computed numerically. In addition, the characteristic fields are neither genuinely nonlinear nor linearly degenerate, hence the determination of the viscosity coefficients in flux-vector splitting schemes becomes a non-trivial task. In any case we have shown that SPEC-INT gives a good resolution on the numerical approximation with a relative small number of mesh points, hence it is competitive with respect to the simpler component-wise

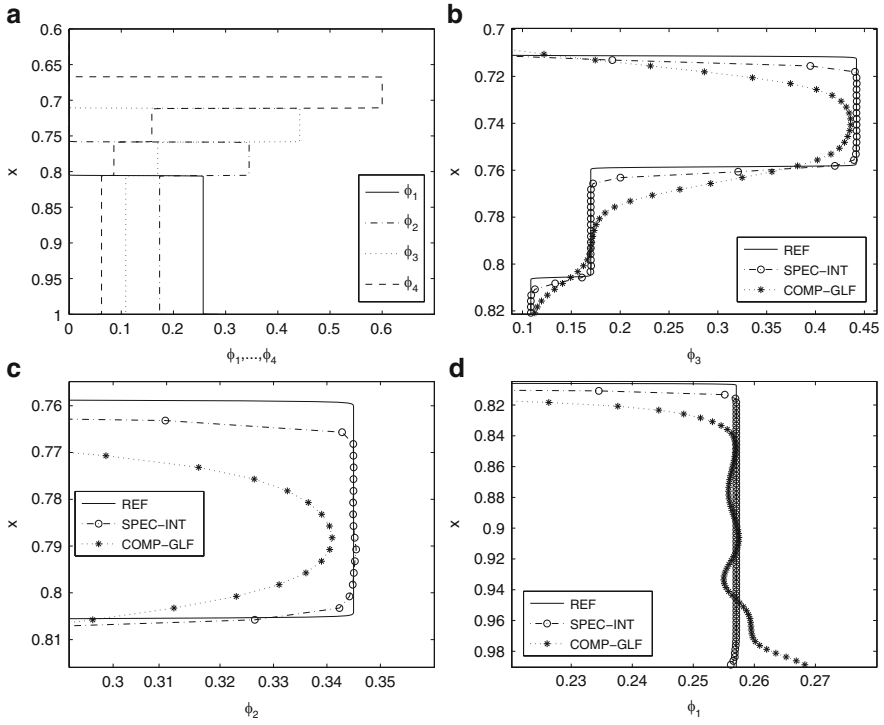

Fig. 10 Example 6: reference solution for $\phi_1, \ldots, \phi_4$ and ϕ computed by SPEC-INT with $M_{\text{ref}} = 6{,}400$ (**a**, **b**), and details of numerical solutions with $M = 400$ (**c**–**f**), at $t = 300$ s.

schemes. In recent work [30] it is shown that SPEC-INT is even more competitive than cheaper component-wise schemes, such as COMP-GLF, in an Adaptive Mesh Refinement (AMR) framework, since its non-oscillatory properties will help to avoid unnecessary refinement in regions of constant concentration.

5 Multidimensional Models

5.1 Adaptive Multiresolution (MR) Techniques

Adaptive multiresolution (MR) techniques are naturally fitted for FV schemes [13, 54, 69, 77]. They are based on representing the numerical solution on a fine grid by values on a much coarser grid plus a series of differences at different levels of nested dyadic grids. These differences are small in regions where the solution is smooth. Therefore, by discarding small details (the so-called "thresholding" operation), data compression can be achieved [13]. This automatic grid

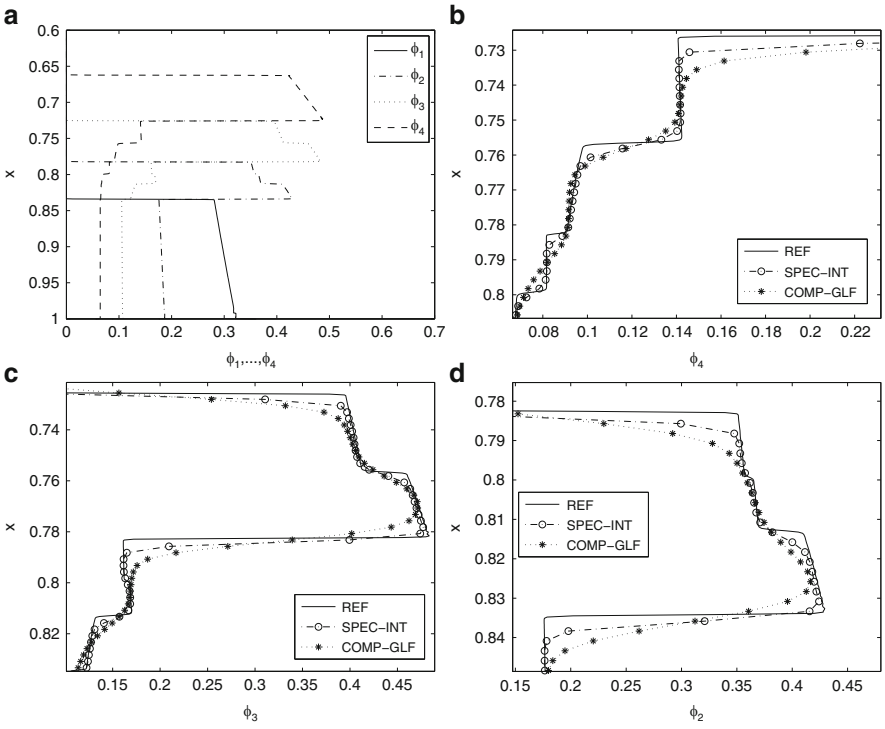

Fig. 11 Example 7: numerical solution for $\phi_1, \ldots, \phi_4$ with $M = 400$: at $t = 250\,\mathrm{s}$ (**a**) and enlarged views (**b–d**), where the reference solution is computed using SPEC-INT with $M_{\mathrm{ref}} = 6{,}400$

refinement allows for memory and CPU time reductions while the approximation error remains controlled. The governing equations, in the present case (15) and (16), are discretized with a classical FV discretization. This approach has been implemented in [28] for (15) and (16) with $A \equiv 0$ and $\nu = 0$ to simulate the settling of a monodisperse suspension in a tilted narrow channel, which gives rise to the so-called "Boycott effect" [14], namely an increase of settling rates compared with a vertical channel. This effect is related to the formation of discontinuities in u and a boundary layer beneath a downward-facing inclined wall, occurs in vessels of simple geometry, and is therefore suitable for testing the capability of adaptive methods to concentrate computational effort on zones of strong variation such as discontinuities in u and boundary layers. In [28] the MR technique indeed produced a significant gain in efficiency.

Figure 12 (Example 8) shows an example from [28] with $L = 8$ resolution levels in total, corresponding to a finest grid of 256×256 cells on which (16) (with $\nu = 0$, $\lambda = 1, \boldsymbol{k} = (\cos\theta, \sin\theta)$, $\zeta = 0.67$ and $\mu(u) = (1-u)^{-2}$ and pressure stabilization [15]) is solved by a finite volume scheme, while (16) (with $f(u) = u(1-u)^2$ and $A \equiv 0$) is solved on an adaptive grid by the first-order Godunov scheme.

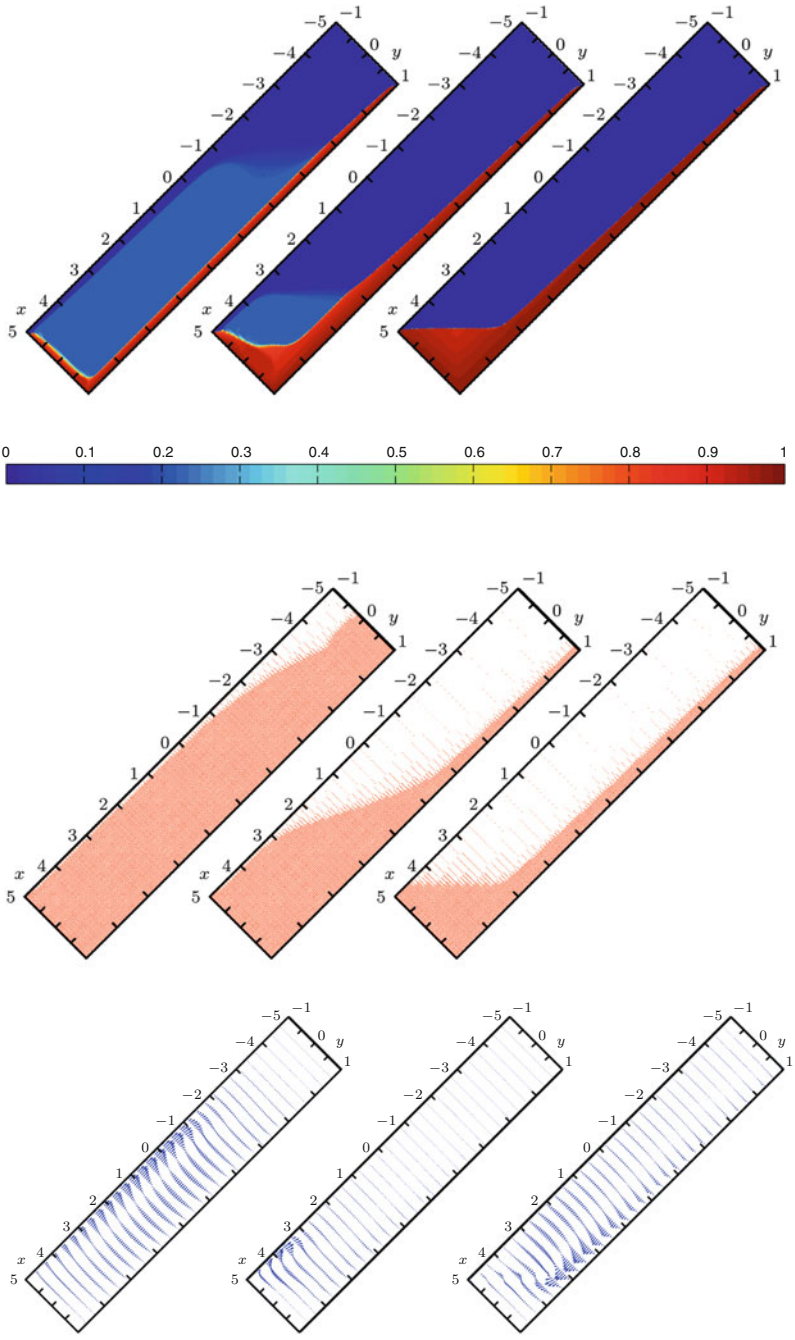

Fig. 12 Example 8: simulation of the settling of a suspension of constant initial concentration $u_0 = 0.2$ in a channel inclined by $\theta = 45°$ [28]. *Top*: concentration u, *middle*: leaves of the adaptive tree, *bottom*: velocity $\boldsymbol{v}$, at times $t = 1.5$ (*left*), $t = 3.75$ (*middle*), and $t = 11.25$ (*right*). We have $\|\boldsymbol{v}(1.5)\| = 11.84$, $\|\boldsymbol{v}(3.75)\| = 3.72$ and $\|\boldsymbol{v}(11.25)\| = 2.7 \times 10^{-2}$

5.2 *Finite Volume Element (FVE) Methods*

If $A \not\equiv 0$ and $A(\cdot)$ has the behaviour (10), then (15) becomes strongly degenerate parabolic. Usually the type-change interface $u = u_c$ is associated with a discontinuity in the solution. An open problem of interest in applications is the development of numerical methods for (15) and (16) under the assumption of strong degeneracy. While FV methods are the best choice to discretize (15) (due to its convection-dominated nature along with the strong gradients in the solution), they are outperformed by finite element (FE) methods for what concerns the discretizations of the momentum and continuity equations forming the Stokes equations [31]. This observation motivated the FVE method (cf. [73] and the references cited in that paper) as a "hybrid" methodology, which is intermediate between FV and FE methods: the method is locally conservative (like a classical FV method) while it allows for L^2 estimates in a rather natural way (as in classical FE methods). The basic idea is to reformulate the FE scheme as a FV scheme on a dual mesh (see [4, 73] for details). The FVE methodology permits treating the full system (15) and (16) by a unified approach.

This method is implemented in [29] for a 2D section of an axisymmetric vessel (which requires cylindrical coordinates, cf., e.g., [9,52]), $\nu = 0$ (the Stokes system), and pointwise degeneracy ($a(u) = 0$ at $u = 0$ and $u = u_{\max}$ only). The last restriction was found necessary since the particular Galerkin discretization used in [29] relies on formulas like $\Delta A(u) = \nabla \cdot (a(u)\nabla u)$ which are not valid in general in the strongly degenerate case. However, numerical solutions behave reasonably in both the pointwise and strongly degenerate cases.

As a numerical example, we consider the fill-up of a cylindrical settling tank with a so-called skirt baffle and circumferential suction lifts introduced in [61, 92]. The essential parameters are $\rho_s - \rho_f = 1{,}562\,\mathrm{kg/m^3}$, $f(u) = 2.2 \times 10^{-3} u(1 - u/0.9)^2\,\mathrm{m/s}$, $u_{\text{in}} = 0.1$, $g = 9.81\,\mathrm{m/s^2}$, $v_{z,\text{out}} = \nu v_{z,\text{in}}$, $v_{r,\text{ofl}} = \frac{9-\nu}{52} v_{z,\text{in}}$, $v_{r,\text{in}} = 0.019\,\mathrm{m/s}$ and $\Delta t = 5\,\mathrm{s}$. The primal mesh $\mathcal{T}$ is composed of 7,410 elements and 4,206 interior nodes. The boundary conditions for velocity at the suction lifts are given by $\boldsymbol{v} = (0, -u_{z,\text{out}}/4)$, where $v_{z,\text{out}} = \nu v_{r,\text{in}}$. See Figs. 13 and 14 for numerical results.

6 Alternate Treatments and Some Open Problems

Concerning the analysis of TVD and FTVD schemes of Sect. 2, we mention that in [20] an entropy inequality similar to (31) was used to prove that the first-order version of our scheme converges to a unique entropy solution of the conservation law. Although our numerical experiments indicate that the second-order schemes STVD and FTVD also converge to the unique entropy solution, the entropy inequality (31) is not quite in a form that allows us to repeat the uniqueness argument in [20]. We leave this as an open problem.

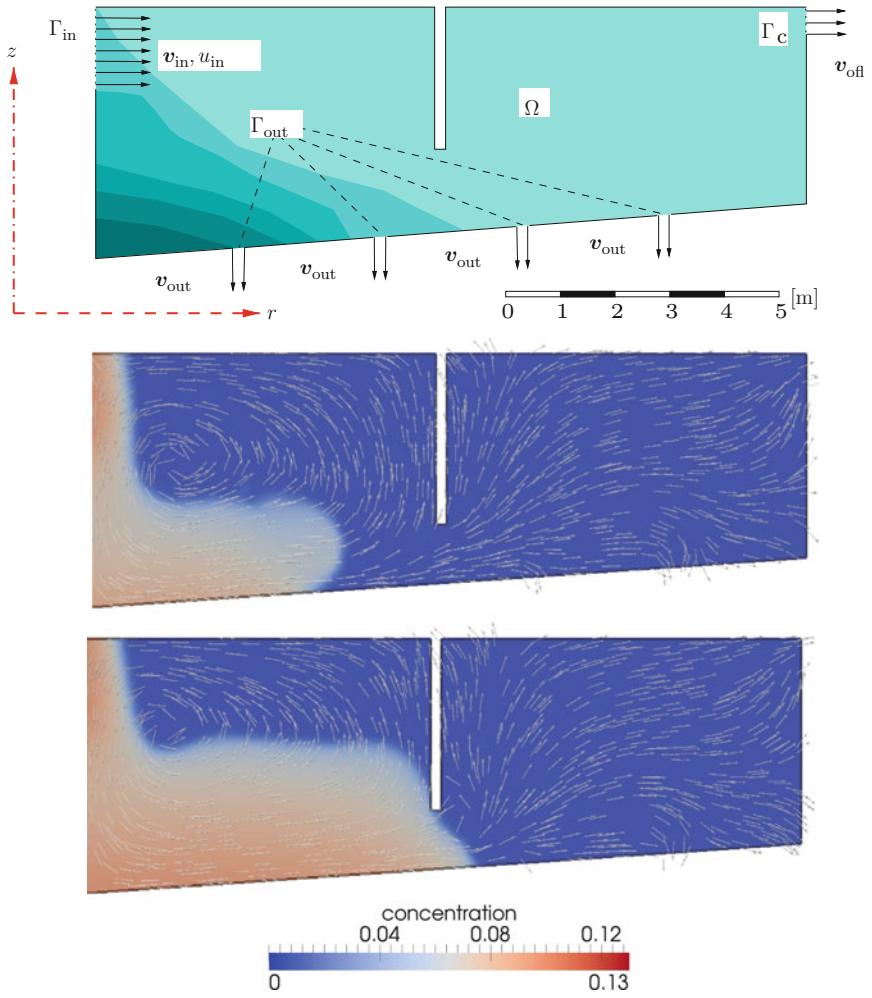

Fig. 13 Numerical simulation of the fill-up of a settling basin with skirt baffle (*top*) showing the solids concentration u at $t = 500$ s (*middle*) and 1,000 s (*bottom*)

Let us mention some of the works that analyze problems related to the conservation law with discontinuous flux (11) analyzed in Sect. 3. Another spatially one-dimensional, nonlocal sedimentation model was studied by Sjögreen et al. [82], who consider a hyperbolic-elliptic model problem given by (1) coupled with $-\eta(v_{\text{s}})_{xx} + v_{\text{s}} = u$, where $\eta > 0$ is a viscosity parameter. Clearly, at any fixed position x_0, $v_{\text{s}}(x_0, t)$ will depend on $u(\cdot, t)$ as a whole; the nonlocal dependence is not limited to a neighborhood, as in [99] and herein. They prove that their model has a smooth solution, and present numerical solutions obtained by a high-order difference scheme. Furthermore, the (local) kinematic model of sedimentation (2) is similar to the well-known Lighthill-Whitham-Richards (LWR) model of

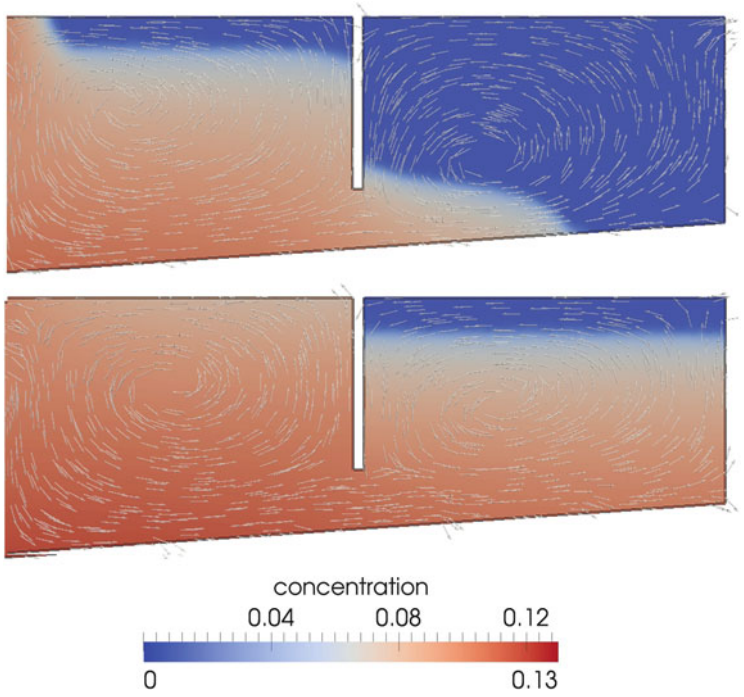

Fig. 14 Continuation of Fig. 13 showing the solids concentration u at $t = 2{,}000\,\mathrm{s}$ (*top*) and $7{,}500\,\mathrm{s}$ (*bottom*)

vehicular traffic. Sopasakis and Katsoulakis [83] extended the LWR model to a nonlocal version by a "look-ahead" rule, i.e. drivers choose their velocity taking account the density on a stretch of road ahead of them. Kurganov and Polizzi [63] showed that an extension of the well-known Nesshayu-Tadmor (NT) central nonoscillatory scheme [71] is suitable for the nonlocal model of [83], which can be written as (11) for $\alpha = 1$ and $V(w) = \exp(-w)$, and if we replace K_a by a particular non-symmetric kernel function with compact support. Related models with a nonlocal convective flux that have been analyzed within an entropy solution framework (as done herein and in [12]) include the continuum model for the flow of pedestrians by Hughes [57], which gives rise to a multi-dimensional conservation law with a nonlocal flux; see also [36, 39]. See [12] for further applications.

As another open research problem, a systematic travelling wave analysis of (11), which would extend the results of [99], is still lacking. Such an analysis could explain whether new phenomena, e.g. nonclassical shocks, should be expected when one considers the formal limit $a \to 0$ of entropy solutions of (11), especially in the case $\alpha \geq 1$. Unfortunately, most of the constants appearing in the compactness estimates of [12] are not uniform, i.e. they blow up when $a \to 0$. It is therefore not clear whether a sequence of entropy solutions converges to a meaningful limit as $a \to 0$. This problem should at first be explored numerically.

Related to the multiresolution (MR) method for tackling the multi-dimensional system (15) and (16) outlined in Sect. 5, we mention that in [28] MR was applied to the solution of (15) (with $A \equiv 0$) only, but the more involved Stokes system was always solved on the finest grid. The MR approach of [28] should be extended to a method that solves both (15) and (16) (first, for the Stokes system ($\nu = 0$), and then for the Navier-Stokes case) on an adaptively refined grid. Further speed-up of adaptive methods is achieved using local time stepping strategies [70]. The central tasks are the implementation and numerical analysis of pressure stabilization techniques and of projection schemes to take into account the incompressibility of $\boldsymbol{v}$ (cf., e.g., [53, 78]). Further research will concern the polydisperse case, for which (15) will be replaced by a system of conservation laws. Finally, concerning the FVE method described in Sect. 5.2, besides incorporating the full Navier-Stokes terms, one should modify the FVE scheme so that its formulation from the onset also covers the strongly degenerate case. Thus, discretizations alternative to the Discontinuous Galerkin (DG) formulation employed in [29] should be tested by adequately choosing the numerical flux associated with (15), and we intend to investigate whether the choice of a diamond mesh (one of the dual meshes) made in [29] will in general capture the hyperbolic-parabolic transition.

Acknowledgements RB acknowledges support by Fondecyt project 1090456 and BASAL project CMM, Universidad de Chile and Centro de Investigación en Ingeniería Matemática (CI^{2}MA), Universidad de Concepción. RR is supported by ERC advanced grant 227058, project *Mathcard, Mathematical Modelling and Simulation of the Cardiovascular System*. HT is supported by Fondecyt project 11110264, and RB and HT are funded by CONICYT project Anillo ACT1118 (ANANUM). CV is supported by Universidad del Norte, project 2012-002.

References

1. J. Anderson, A secular equation for the eigenvalues of a diagonal matrix perturbation. Linear Algebra Appl. **246**, 49–70 (1996)
2. B. Andreianov, K.H. Karlsen, N.H. Risebro, A theory of L^1-dissipative solvers for scalar conservation laws with discontinuous flux. Arch. Ration. Mech. Anal. **201**, 27–86 (2011)
3. D.P. Ballou, Solutions to non-linear hyperbolic Cauchy problems without convexity conditions. Trans. Am. Math. Soc. **152**, 441–460 (1970)
4. R.E. Bank, D.J. Rose, Some error estimates for the box method. SIAM J. Numer. Anal. **24**, 777–787 (1987)
5. G.K. Batchelor, Sedimentation in a dilute polydisperse system of interacting spheres. Part 1. General theory. J. Fluid Mech. **119**, 379–408 (1982)
6. G.K. Batchelor, R.W.J. van Rensburg, Structure formation in bidisperse sedimentation. J. Fluid Mech. **166**, 379–407 (1986)
7. G.K. Batchelor, C.S. Wen, Sedimentation in a dilute polydisperse system of interacting spheres. Part 2. Numerical results. J. Fluid Mech. **124**, 495–528 (1982)
8. S. Benzoni-Gavage, R.M. Colombo, An n-populations model for traffic flow. Eur. J. Appl. Math. **14**, 587–612 (2003)
9. C. Bernardi, M. Dauge, Y. Maday, *Spectral Methods for Axisymmetric Domains* (Gauthier-Villars, Paris, 1999)

10. S. Berres, R. Bürger, K.H. Karlsen, E.M. Tory, Strongly degenerate parabolic-hyperbolic systems modeling polydisperse sedimentation with compression. SIAM J. Appl. Math. **64**, 41–80 (2003)
11. A.L. Bertozzi, T. Laurent, J. Rosado, L^p theory for the multidimensional aggregation equation. Commun. Pure Appl. Math. **64**, 45–83 (2011)
12. F. Betancourt, R. Bürger, K.H. Karlsen, E.M. Tory, On nonlocal conservation laws modelling sedimentation. Nonlinearity **24**, 855–885 (2011)
13. B.L. Bihari, A. Harten, Multiresolution schemes for the numerical solution of 2-D conservation laws I. SIAM J. Sci. Comput. **18**, 315–354 (1997)
14. A.E. Boycott, Sedimentation of blood corpuscles. Nature **104**, 532 (1920)
15. F. Brezzi, J. Pitkäranta, On the stabilization of finite element approximations of the Stokes equations, in *Efficient Solutions of Elliptic Systems*, Kiel. Notes on Numerical Fluid Mechanics, vol. 10 (Vieweg, Braunschweig, 1984), pp. 11–19
16. R. Bürger, K.H. Karlsen, Conservation laws with discontinuous flux: a short introduction. J. Eng. Math. **60**, 241–247 (2008)
17. R. Bürger, W.L. Wendland, Sedimentation and suspension flows: historical perspective and some recent developments. J. Eng. Math. **41**, 101–116 (2001)
18. R. Bürger, K.H. Karlsen, E.M. Tory, W.L. Wendland, Model equations and instability regions for the sedimentation of polydisperse suspensions of spheres. ZAMM Z. Angew. Math. Mech. **82**, 699–722 (2002)
19. R. Bürger, K.H. Karlsen, N.H. Risebro, J.D. Towers, Monotone difference approximations for the simulation of clarifier-thickener units. Comput. Vis. Sci. **6**, 83–91 (2004)
20. R. Bürger, K.H. Karlsen, N.H. Risebro, J.D. Towers, Well-posedness in BV_t and convergence of a difference scheme for continuous sedimentation in ideal clarifier-thickener units. Numer. Math. **97**, 25–65 (2004)
21. R. Bürger, K.H. Karlsen, J.D. Towers, A mathematical model of continuous sedimentation of flocculated suspensions in clarifier-thickener units. SIAM J. Appl. Math. **65**, 882–940 (2005)
22. R. Bürger, A. García, K.H. Karlsen, J.D. Towers, A family of numerical schemes for kinematic flows with discontinuous flux. J. Eng. Math. **60**, 387–425 (2008)
23. R. Bürger, K.H. Karlsen, J.D. Towers, An Engquist-Osher type scheme for conservation laws with discontinuous flux adapted to flux connections. SIAM J. Numer. Anal. **47**, 1684–1712 (2009)
24. R. Bürger, R. Donat, P. Mulet, C.A. Vega, Hyperbolicity analysis of polydisperse sedimentation models via a secular equation for the flux Jacobian. SIAM J. Appl. Math. **70**, 2186–2213 (2010)
25. R. Bürger, K.H. Karlsen, H. Torres, J.D. Towers, Second-order schemes for conservation laws with discontinuous flux modelling clarifier-thickener units. Numer. Math. **116**, 579–617 (2010)
26. R. Bürger, R. Donat, P. Mulet, C.A. Vega, On the implementation of WENO schemes for a class of polydisperse sedimentation models. J. Comput. Phys. **230**, 2322–2344 (2011)
27. R. Bürger, R. Donat, P. Mulet, C.A. Vega, On the hyperbolicity of certain models of polydisperse sedimentation. Math. Methods Appl. Sci. **35**, 723–744 (2012)
28. R. Bürger, R. Ruiz-Baier, K. Schneider, H. Torres, A multiresolution method for the simulation of sedimentation in inclined channels. Int. J. Numer. Anal. Model. **9**, 479–504 (2012)
29. R. Bürger, R. Ruiz-Baier, H. Torres, A stabilized finite volume element formulation for sedimentation-consolidation processes. SIAM J. Sci. Comput. **34**, B265–B289 (2012)
30. R. Bürger, P. Mulet, L.M. Villada, Spectral WENO schemes with adaptive mesh refinement for models of polydisperse sedimentation. ZAMM Z. Angew. Math. Mech. **93**, 373–386 (2013)
31. E. Burman, A. Quarteroni, B. Stamm, Interior penalty continuous and discontinuous finite element approximations of hyperbolic equations. J. Sci. Comput. **43**, 293–312 (2010)
32. M.C. Bustos, F. Concha, On the construction of global weak solutions in the Kynch theory of sedimentation. Math. Method Appl. Sci. **10**, 245–264 (1988)
33. M.C. Bustos, F. Concha, R. Bürger, E.M. Tory, *Sedimentation and Thickening. Phenomenological Foundation and Mathematical Theory* (Kluwer, Dordrecht, 1999)
34. K.S. Cheng, Constructing solutions of a single conservation law. J. Differ. Equ. **49**, 344–358 (1983)

35. H.S. Coe, G.H. Clevenger, Methods for determining the capacity of slime settling tanks. Trans. AIME **55**, 356–385 (1916)
36. R.M. Colombo, M. Herty, M. Mercier, Control of the continuity equation with a non local flow. ESAIM Control Opt. Calc. Var. **17**, 353–379 (2011)
37. A. Coronel, F. James, M. Sepúlveda, Numerical identification of parameters for a model of sedimentation processes. Inverse Probl. **19**, 951–972 (2003)
38. R.H. Davis, H. Gecol, Hindered settling function with no empirical parameters for polydisperse suspensions. AIChE J. **40**, 570–575 (1994)
39. M. Di Francesco, P.A. Markowich, J.-F. Pietschmann, M.-T. Wolfram, On the Hughes' model for pedestrian flow: the one-dimensional case. J. Differ. Equ. **250**, 1334–1362 (2011)
40. S. Diehl, Shock behaviour of sedimentation in wastewater treatment. M. Sc. thesis, University of Lund, Lund (1988)
41. S. Diehl, Estimation of the batch-settling flux function for an ideal suspension from only two experiments. Chem. Eng. Sci. **62**, 4589–4601 (2007)
42. S. Diehl, Shock-wave behaviour of sedimentation in wastewater treatment: a rich problem, in *Analysis for Science, Engineering and Beyond*, ed. by K. Åström et al. (Springer, Berlin, 2012), pp. 175–214
43. R. Donat, P. Mulet, A secular equation for the Jacobian matrix of certain multi-species kinematic flow models. Numer. Methods Partial Differ. Equ. **26**, 159–175 (2010)
44. J.V.N. Dorr, The use of hydrometallurgical apparatus in chemical engineering. J. Ind. Eng. Chem. **7**, 119–130 (1915)
45. A. Einstein, Eine neue Bestimmung der Moleküldimensionen. Ann. Phys. **19**, 289–306 (1906); A. Einstein, Berichtigung zu meiner Arbeit: "Eine neue Bestimmung ...". Ann. Phys. **34**, 591–592 (1911)
46. B. Engquist, S. Osher, One-sided difference approximations for nonlinear conservation laws. Math. Comput. **36**, 321–351 (1981)
47. T. Frising, C. Noïk, C. Dalmazzone, The liquid/liquid sedimentation process: from droplet coalescence to technologically enhanced water/oil emulsion gravity separators: a review. J. Dispers. Sci. Technol. **27**, 1035–1057 (2006)
48. E. Godlewski, P. Raviart, *Numerical Approximation of Hyperbolic Systems of Conservation Laws* (Springer, New York, 1996)
49. S. Gottlieb, C.-W. Shu, E. Tadmor, Strong stability-preserving high-order time discretization methods. SIAM Rev. **43**, 89–112 (2001)
50. P. Grassia, S.P. Usher, P.J. Scales, Closed-form solutions for batch settling height from model settling flux functions. Chem. Eng. Sci. **66**, 964–972 (2011)
51. P. Grassmann, R. Straumann, Entstehen und Wandern von Unstetigkeiten der Feststoffkozentration in Suspensionen. Chem. Ing. Tech. **35**, 477–482 (1963)
52. A. Guardone, L. Vigevano, Finite element/volume solution to axisymmetric conservation laws. J. Comput. Phys. **224**, 489–518 (2007)
53. J.L. Guermond, P. Minev, J. Shen, An overview of projection methods for incompressible flows. Comput. Method Appl. Eng. **195**, 6011–6045 (2006)
54. A. Harten, Multiresolution algorithms for the numerical solution of hyperbolic conservation laws. Commun. Pure Appl. Math. **48**, 1305–1342 (1995)
55. P.G.W. Hawksley, The effect of concentration on the settling of suspensions and flow through porous media, in *Some Aspects of Fluid Flow* (E. Arnold, London, 1951), pp. 114–135
56. K. Höfler, S. Schwarzer, The structure of bidisperse suspensions al low Reynolds numbers, in *Multifield Problems: State of the Art*, ed. by A.M. Sändig, W. Schiehlen, W.L. Wendland (Springer, Berlin, 2000), pp. 42–49
57. R.L. Hughes, A continuum theory for the flow of pedestrians. Transp. Res. B **36**, 507–535 (2002)
58. K.H. Karlsen, N.H. Risebro, On the uniqueness and stability of entropy solutions for nonlinear degenerate parabolic equations with rough coefficients. Discret. Contin. Dyn. Syst. **9**, 1081–1104 (2003)

59. K.H. Karlsen, N.H. Risebro, J.D. Towers, Upwind difference approximations for degenerate parabolic convection-diffusion equations with a discontinuous coefficient. IMA J. Numer. Anal. **22**, 623–664 (2002)
60. K.H. Karlsen, N.H. Risebro, J.D. Towers, L^1 stability for entropy solutions of nonlinear degenerate parabolic convection-diffusion equations with discontinuous coefficients. Skr. K. Nor. Vid. Selsk (3), 1–49 (2003)
61. D. Kleine, B.D. Reddy, Finite element analysis of flows in secondary settling tanks. Int. J. Numer. Methods Eng. **64**, 849–876 (2005)
62. S.N. Kružkov, First order quasilinear equations in several independent variables. Math. USSR Sb. **10**, 217–243 (1970)
63. A. Kurganov, A. Polizzi, Non-oscillatory central schemes for traffic flow models with Arrhenius look-ahead dynamics. Netw. Heterog. Media **4**, 431–451 (2009)
64. G.J. Kynch, A theory of sedimentation. Trans. Farad. Soc. **48**, 166–176 (1952)
65. M.J. Lockett, K.S. Bassoon, Sedimentation of binary particle mixtures. Powder Technol. **24**, 1–7 (1979)
66. G. Loeper, Uniqueness of the solution of the Vlasov-Poisson system with bounded density. J. Math. Pures Appl. **86**, 68–79 (2006)
67. T.P. Liu, Invariants and asymptotic behavior of solutions of a conservation law. Proc. Am. Math. Soc. **71**, 227–231 (1978)
68. J.H. Masliyah, Hindered settling in a multiple-species particle system. Chem. Eng. Sci. **34**, 1166–1168 (1979)
69. S. Müller, *Adaptive Multiscale Schemes for Conservation Laws* (Springer, Berlin, 2003)
70. S. Müller, Y. Stiriba, Fully adaptive multiscale schemes for conservation laws employing locally varying time stepping. J. Sci. Comput. **30**, 493–531 (2007)
71. H. Nessyahu, E. Tadmor, Non-oscillatory central differencing for hyperbolic conservation laws. J. Comput. Phys. **87**, 408–463 (1990)
72. V.S. Patwardhan, C. Tien, Sedimentation and liquid fluidization of solid particles of different sizes and densities. Chem. Eng. Sci. **40**, 1051–1060 (1985)
73. A. Quarteroni, R. Ruiz-Baier, Analysis of a finite volume element method for the Stokes problem. Numer. Math. **118**, 737–764 (2011)
74. H.-K. Rhee, R. Aris, N.R. Amundson, *First-Order Partial Differential Equations*. Volume 1: Theory and Applications of Single Equations (Prentice Hall, Englewood Cliffs, 1986)
75. J.F. Richardson, W.N. Zaki, Sedimentation and fluidization: part I. Trans. Instn. Chem. Eng. (Lond.) **32**, 35–53 (1954)
76. F. Rosso, G. Sona, Gravity-driven separation of oil-water dispersions. Adv. Math. Sci. Appl. **11**, 127–151 (2001)
77. K. Schneider, O. Vasilyev, Wavelet methods in computational fluid dynamics. Ann. Rev. Fluid Mech. **42**, 473–503 (2010)
78. L. Shen, Z. Chen, Analysis of a stabilized finite volume method for the transient Stokes equations. Int. J. Numer. Anal. Model. **6**, 505–519 (2009)
79. C.-W. Shu, High order weighted essentially nonoscillatory schemes for convection dominated problems. SIAM Rev. **51**, 82–126 (2009)
80. C.-W. Shu, S. Osher, Efficient implementation of essentially non-oscilatory shock capturing schemes. J. Comput. Phys. **77**, 439–471 (1988)
81. D.B. Siano, Layered sedimentation in suspensions of monodisperse spherical colloidal particles. J. Colloid Interface Sci. **68**, 111–127 (1979)
82. B. Sjögreen, K. Gustavsson, R. Gudmundsson, A model for peak formation in the two-phase equations. Math. Comput. **76**, 1925–1940 (2007)
83. A. Sopasakis, M.A. Katsoulakis, Stochastic modelling and simulation of traffic flow: asymmetric single exclusion process with Arrhenius look-ahead dynamics. SIAM J. Appl. Math. **66**, 921–944 (2006)
84. H.H. Steinour, Rate of sedimentation. Nonflocculated suspensions of uniform spheres. Ind. Eng. Chem. **36**, 618–624 (1944)

85. G. Strang, On the construction and comparison of difference schemes. SIAM J. Numer. Anal. **5**, 506–517 (1968)
86. P.K. Sweby, High resolution schemes using flux limiters for hyperbolic conservation laws. SIAM J. Numer. Anal. **21**, 995–1011 (1984)
87. B. Temple, Global solution of the Cauchy problem for a class of 2×2 nonstrictly hyperbolic conservation laws. Adv. Appl. Math. **3**, 335–375 (1982)
88. J.D. Towers, A difference scheme for conservation laws with a discontinuous flux: the nonconvex case. SIAM J. Numer. Anal. **39**, 1197–1218 (2001)
89. V. Vand, Viscosity of solutions and suspensions. I. Theory. J. Phys. Chem. **52**, 277–299 (1948)
90. G.B. Wallis, A simplified one-dimensional representation of two-component vertical flow and its application to batch sedimentation, in *Proceedings of the Symposium on the Interaction Between Fluids and Particles*, London, 20–22 June 1962 (Institution of Chemical Engineers, London, 1962), pp. 9–16
91. G.B. Wallis, *One-Dimensional Two-Phase Flow* (McGraw-Hill, New York, 1969)
92. R.W. Watts, S.A. Svoronos, B. Koopman, One-dimensional modeling of secondary clarifiers using a concentration and feed velocity-dependent dispersion coefficient. Water Res. **30**, 2112–2124 (1996)
93. R.H. Weiland, Y.P. Fessas, B.V. Ramarao, On instabilities arising during sedimentation of two-component mixtures of solids. J. Fluid Mech. **142**, 383–389 (1984)
94. A.J. Wilson, *The Living Rock* (Woodhead Publishing, Cambridge, 1994)
95. G.C.K. Wong, S.C.K. Wong, A multi-class traffic flow model—an extension of LWR model with heterogeneous drivers. Transp. Res. A **36**, 827–841 (2002)
96. A. Zeidan, S. Rohani, A. Bassi, P. Whiting, Review and comparison of solids settling velocity models. Rev. Chem. Eng. **19**, 473–530 (2003)
97. M. Zhang, C.-W. Shu, G.C.K. Wong, S.C. Wong, A weighted essentially non-oscillatory numerical scheme for a multi-class Lighthill-Whitham-Richards traffic flow model. J. Comput. Phys. **191**, 639–659 (2003)
98. P. Zhang, R.X. Liu, S.C. Wong, S.Q. Dai, Hyperbolicity and kinematic waves of a class of multi-population partial differential equations. Eur. J. Appl. Math. **17**, 171–200 (2006)
99. K. Zumbrun, On a nonlocal dispersive equation modeling particle suspensions. Q. Appl. Math. **57**, 573–600 (1999)